NOAA Technical Report ERL 420-WPL 56

# Analysis Methods for Narrow-Beam High-Frequency Radar Sea Echo

Belinda J. Lipa
Donald E. Barrick

April 1982

**U.S. DEPARTMENT OF COMMERCE**
National Oceanic and Atmospheric Administration
Environmental Research Laboratories

NOAA Technical Report ERL 420-WPL 56

# Analysis Methods for Narrow-Beam High-Frequency Radar Sea Echo

Belinda J. Lipa
Donald E. Barrick

Wave Propagation Laboratory
Boulder, Colorado

April 1982

**U.S. Department of Commerce**
Malcolm Baldrige, Secretary

National Oceanic and Atmospheric Administration
John V. Byrne, Administrator

Environmental Research Laboratories
Boulder, Colorado
George H. Ludwig, Director

## NOTICE

Mention of a commercial company or product does not constitute an endorsement by NOAA Environmental Research Laboratories. Use for publicity or advertising purposes of information from this publication concerning proprietary products or the tests of such products is not authorized.

# CONTENTS

As more advanced versions of the computer programs contained herein evolve, the authors will be happy to forward them to interested users. Please write to either author if you wish to be put on a mailing list for future program listings.

# Analysis Methods for Narrow-Beam High-Frequency Radar Sea Echo

**Belinda J. Lipa*** **and Donald E. Barrick**

ABSTRACT. The analysis of high-frequency (HF) radar sea echo is based on the interpretation of the echo power spectrum in terms of Barrick's equations for the radar cross section, to give parameters of the ocean wave, wind, and current-velocity fields. To provide an analysis of these equations, which are straightforward but mathematically complex and not generally well understood, a detailed review of analytical and computational techniques for application to narrow-beam radars (both one and two beams) is presented. Steps are given and a computer program is supplied for the 'forward' calculation, i.e., the calculation of the radar Doppler spectrum corresponding to a model of the directional ocean waveheight spectrum. The 'reverse' problem is then considered, and the derivation of ocean-surface parameters from the radar data, using least-squares estimation techniques, is described. First, methods for estimating the ocean waveheight, the dominant wave period, wave direction, and wave beamwidth from the energy and centroid frequency of the dominant peaks in the radar spectrum are shown. Since these four parameters are relatively insensitive to moderate frequency smearing that may occur as a result of ionospheric motion, the methods described are particularly suited to the analysis of skywave radar data. Then, methods for use with higher quality data are described, using the total radar spectrum to give the longer-period (>8-s) ocean-wave nondirectional spectrum, as well as the direction and beamwidth as a function of ocean-wave frequency. Statistical tests are discussed that can be used to assess the quality of the model fit and to place confidence limits on the derived parameters. These techniques are illustrated by application to simulated data for both single- and double-beam radar systems. It is shown that the amount of directional information available from a single-beam radar is somewhat limited; for example, ocean-wave parameters as a function of ocean-wave frequency cannot be derived unless the wave direction is almost perpendicular to the radar beam. The two-beam system, however, gives good statistical accuracy for the wave parameters at all wave directions. Meant to serve as a manual for a variety of users of surface-wave and skywave HF narrow-beam radars, the document is self contained. All equations necessary for application to sea echo are given and explained and references to earlier sources and derivations are cited as further background for the reader. Several mathematical results and techniques presented here have not appeared elsewhere. All essential computer programs (coded in FORTRAN) required to implement these methods are provided and explained; samples of input/output for user verification are included.

---

* Codar Research, Woodside, California; work performed under NOAA Contract No. NA82RAC00010.

# 1. INTRODUCTION

Over the past ten years, several groups have demonstrated the unique capability of HF radar for the remote sensing of ocean-surface waves, winds, and currents. The strength of this method lies in the exact theoretical formulation developed by Barrick (1972a,b), which gives the power spectrum of HF radar sea echo in terms of the directional ocean-wave spectrum and the surface-current velocity. Ocean-surface parameters can therefore be derived by interpretation of these relationships without resort to empirical means.

On the basis of the width of the antenna beam, two types of HF radar systems may be identified. One class includes narrow-beam systems, which were the first radar systems that evolved; the radars first used to observe sea echo were built for military target detection, and hence had narrow beamwidths. Sea echo observed by such systems is also easy to interpret mathematically, as we shall demonstrate. Today, narrow-beam radar systems are employed both in surface and skywave modes. The amount of ocean-surface directional information available from a single beam is quite limited; for this reason two beams inclined at a finite angle are sometimes used when sea-surface conditions can be considered statistically the same in both areas observed. A disadvantage of narrow-beam radars is their large physical size; it is mainly for this reason that a second class of radar systems is under development: small transportable systems that rely on novel antenna design concepts to provide additional directional information.

In the future, most of our efforts will be in the development of broad-beam systems of the second class; therefore, it seems appropriate at this point to document here details of analytical and computational techniques we have developed for use with narrow-beam systems.

At high frequency (HF), the dominant scatter mechanism is Bragg reflection from the ocean surface; the resulting Doppler spectrum consists of prominent peaks caused by first-order scatter, surrounded by a structured higher-order continuum. In sec. 2, we give a theoretical description of narrow-beam radar sea-echo Doppler spectra using Barrick's equations for the first- and second-order radar cross sections. In sec. 3, we show how to reduce the

integral equation for the second-order radar cross section to a convenient nondimensional form. Computer programs are included to calculate the radar spectrum for a model ocean-wave spectrum. Examples of computed spectra are used to illustrate the sensitivity of the radar spectrum to changing ocean-wave conditions. Section 4 describes techniques for the estimation of ocean-wave parameters from narrow-beam radar Doppler spectra. (We have already given general inversion methods in the literature; see, for example, Lipa and Barrick [1980] and Lipa et al. [1981].) We also discuss least-squares estimation methods for use with both single and double radar beams. Parameters of the directional waveheight spectrum are obtained by fitting cardioid ocean-wave spectral models to the radar data. First, we consider a single, dominant ocean wavelength and derive ocean waveheight and the dominant wave period, direction, and beamwidth using as input data the energies and centroid frequencies of the first and second-order radar spectral peaks. Second, we consider a range of long ocean wavelengths and solve for the nondirectional spectrum, and the wave direction and beamwidth also as functions of ocean-wave frequency. Simple grid-search techniques are used to derive the optimum model parameters; computer programs for the generation of grid-search elements are supplied.

The calculation of parameter uncertainties is an important but often neglected aspect of any data analysis program. We describe statistical tests to determine whether or not the ocean-wave spectral model adequately fits the radar data and to place confidence limits on the derived parameters. Although standard, these techniques do not appear to be used at present by either the remote-sensing or the oceanographic communities. The methods are illustrated by application to simulated data for both one-beam and two-beam radars.

## 2. THE RADAR SPECTRUM

Figure 1 shows a typical, measured HF Doppler spectrum of radar echo backscattered near grazing incidence from the sea at 15 MHz. The dominant contribution is produced by first-order scatter from specific spectral components of the ocean wavefield. These surface-height spectral components are termed 'Bragg waves'; their wavelength is exactly one-half the radar wavelength, and they move directly toward or away from the radar station. These

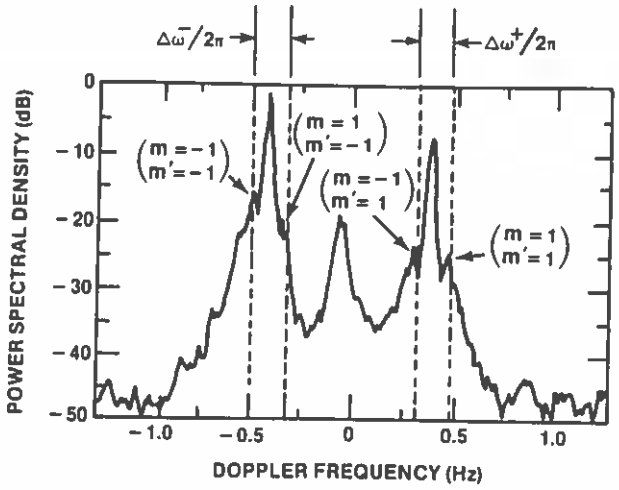


Figure 1.--An 84-sample sea-echo power spectrum recorded by the SRI skywave radar on 17 May 1978, 1628 UT at 15 MHz. The first-order (Bragg) peaks occur at ±0.395 Hz. The dashed lines indicate the positions of the four second-order peaks produced by 12-s swell. The displacements $\Delta\omega^+$ and $\Delta\omega^-$ are used in the text to calculate swell parameters. The theoretical expressions employ definitions of the four swell peaks in terms of $m, m' = \pm 1$.

peaks are evident in fig. 1; their amplitude is two orders of magnitude higher than the surrounding continuum, from which they are separated by well-defined nulls. In the absence of ocean current, the first-order peaks occur at frequencies that depend only on the radar transmitter frequency. The presence of a current or ionospheric layer motion (in the case of skywave radar) causes the whole spectrum to be biased in frequency. The surrounding continuum is due to higher-order scatter, the greater part of which arises from second-order interaction between pairs of ocean waves constituting the total ocean wavefield. It is from the interpretation of this portion of the spectrum (normalized by the first-order energy) that we derive the directional ocean waveheight spectrum. The random appearance of the radar spectrum is due to the random height of the wavetrains composing the surface of the sea. The scatter of the resulting spectral points is described by a $\chi^2$ (chi-squared) distribution with 2N degrees of freedom, where N is the number of spectra averaged (Barrick and Snider, 1977).

## 2.1 First-Order Radar Cross Section

Barrick's equation (1972a) for the first-order radar spectral cross section in the absence of ocean surface current is given by

$$\sigma^{(1)}(\omega) = 2^6 \pi k_o^4 \sum_{m'=\pm 1} S(-2m'\tilde{k}_o)\, \delta(\omega - m'\omega_B) \ , \qquad (1)$$

where $m' = \pm 1$ denotes the sign of the Doppler shift, $\tilde{k}_o$ is the radar wave vector (of magnitude $k_o$ pointing toward the scattering patch), and $S(\cdot)$ is the directional waveheight spectrum. The Bragg resonance condition is imposed by the delta-function constraint. Thus, ideally the first-order peaks are impulse functions at the Bragg frequencies $\pm\omega_B$, defined in terms of the Bragg wavenumber $k_o$ by the dispersion equation

$$\omega_B = \sqrt{2gk_o} \ , \qquad (2)$$

where g is the gravitational acceleration.

In practice, these peaks are broadened somewhat by current turbulence, ionospheric motions (in a skywave radar), and systems effects. In the presence of a surface current (and/or uniform ionospheric motion) the whole spectrum is shifted in frequency by an amount $\delta\omega$ that is proportional to the total radial velocity, $v_{cr}$:

$$\delta\omega = 2v_{cr} k_o \ . \qquad (3)$$

Hence such shifts are readily identified and removed from the data as shown in sec. 4.1. The amplitudes of the first-order peaks are proportional to the directional ocean-wave spectrum at the Bragg wave vectors $\pm 2\tilde{k}_o$. At normal HF frequencies, these correspond to short, saturated waves (e.g., 2-s period for a radar frequency of 25 MHz).

## 2.2 Second-Order Radar Cross Section

Barrick's equation (1972b) for the second-order radar spectral cross section at a Doppler shift $\omega$ is given by

$$\sigma^{(2)}(\omega) = 2^6 \pi k_o^4 \sum_{m,m'=\pm 1} \int_{-\infty}^{\infty} \int_{-\infty}^{\infty} |\Gamma|^2 S(m\tilde{k})\, S(m'\tilde{k}')\, \delta(\omega - m\sqrt{gk} - m'\sqrt{gk'})\, dpdq \ . \qquad (4)$$

Here, the spatial wavenumber p is defined to lie along the radar beam, with q perpendicular. The scattering wave vectors $\tilde{k}$ and $\tilde{k}'$, illustrated in fig. 2,

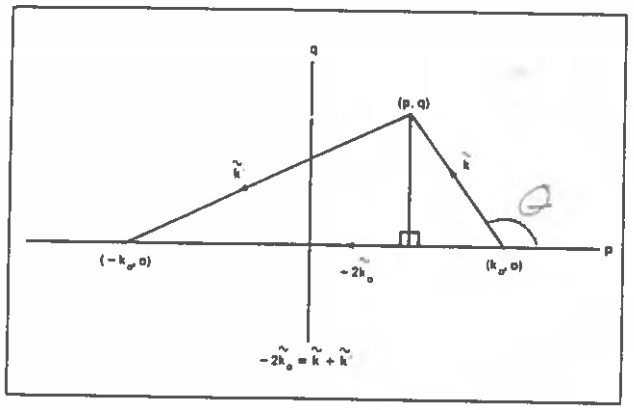


Figure 2.--Illustration of two scattering wave vectors, $\tilde{k}$ and $\tilde{k}'$, producing second-order sea-echo corresponding to integration point (p,q). The perpendicular from (p,q) to the p axis is useful for proving many of the formulae in the text.

are defined by

$$\tilde{k} = (p - k_o, q), \quad \tilde{k}' = (-(p + k_o), -q) , \tag{5}$$

and hence they obey the constraint

$$\tilde{k} + \tilde{k}' = -2\tilde{k}_o . \tag{6}$$

The lengths of the scattering wave vectors are denoted by k and k'. The values of m and m' in (4) take the values +1 and -1, defining the four possible combinations of direction of the two scattering waves. The coupling coefficient $\Gamma$ is given by

$$\Gamma = |\Gamma_H + \Gamma_{EM}| , \tag{7}$$

where $\Gamma_H$ and $\Gamma_{EM}$ are the hydrodynamic and electromagnetic components defined by

$$\Gamma_H = \frac{-i}{2}\left[k + k' - \frac{(kk' - \tilde{k}\cdot\tilde{k}')(\omega^2 + \omega_B{}^2)}{mm'\sqrt{kk'}\,(\omega^2 - \omega_B{}^2)}\right], \tag{8}$$

$$\Gamma_{EM} = \frac{1}{2}\left[\frac{(\tilde{k}\cdot\tilde{k}_o)(\tilde{k}'\cdot\tilde{k}_o)/k_o{}^2 - 2\tilde{k}\cdot\tilde{k}'}{\sqrt{\tilde{k}\cdot\tilde{k}'} + k_o\Delta}\right] . \tag{9}$$

Here $\Delta$ refers to the normalized surface impedance derived by Barrick (1971).

The second-order radar cross section is related to the directional ocean waveheight spectrum through the nonlinear integral equation given in (4). This relationship is not as straightforward as the first-order result, and its study comprises most of the material in this report. We begin by discussing the properties of frequency contours resulting from the second-order Bragg resonance condition for the pairs of ocean waves producing the scatter.

## 2.3 Frequency Contours

Frequency contours are defined by the delta function constraint in (4). They are the loci of the points (p,q) in fig. 2 giving the lengths and directions of the two interacting wave vectors, $\tilde{k}$ and $\tilde{k}'$, that contribute to second-order scatter at a given, constant Doppler frequency. We will now prove that the different combinations of m and m' define disjoint ranges of Doppler frequency.

### 2.3.1 The case $m = m'$

Squaring the argument of the delta function in (4) gives the relation

$$\omega^2 = g(k + k' + 2\sqrt{kk'}) \tag{10}$$

where k and k' are the lengths of the scattering wave vectors. It follows from fig. 2 that because the sum of two sides of a triangle is always greater than the third we have

$$k + k' > 2k_o \ . \tag{11}$$

Since $\sqrt{kk'}$ is positive, it follows from (10) and (11) that

$$\omega^2 > 2gk_o \ . \tag{12}$$

This therefore defines the regions of Doppler frequency outside the Bragg lines; i.e.,

$$\omega > \sqrt{2gk_o} \quad \text{for } m = m' = +1 \tag{13}$$

$$\omega \leq \sqrt{2gk_o} \quad \text{for } m = m' = -1 \ . \tag{14}$$

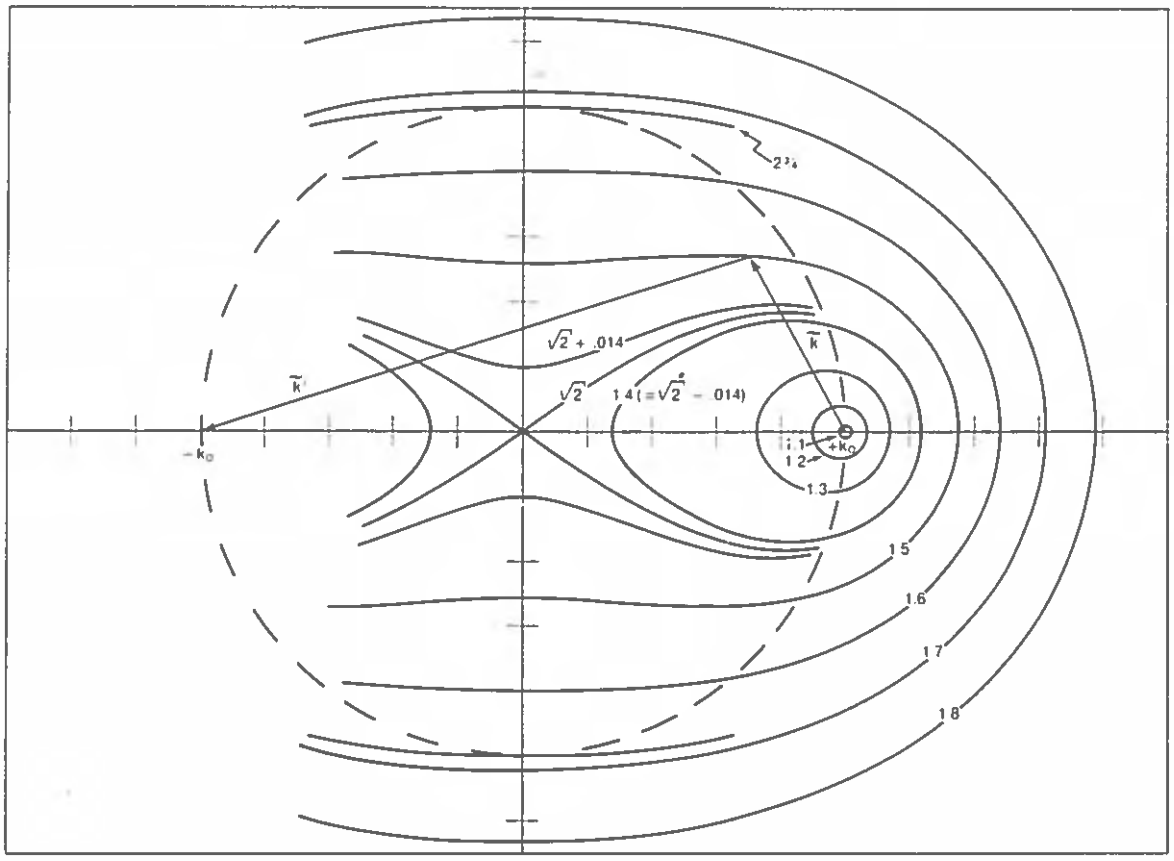


Figure 3.--Normalized constant Doppler frequency contours, $\eta$, vs. wavenumbers, k and k', for the two ocean wave vectors $\tilde{k}$ and $\tilde{k}'$ producing second-order backscatter, for $|\omega| > \omega_B$ (i.e., $m = m'$). Shown is the mathematically singular situation at $|\eta| = \sqrt{2}$, where the two closed contours break apart. The dashed circle shows the electromagnetic 'corner reflector' condition, where k and k' are at right angles ($\tilde{k} \cdot \tilde{k} = 0$); this circle is tangent to the Doppler frequency contour $|\eta| = 2^{3/4}$, producing a mathematical stationarity or peak at this frequency. The contours are symmetric about the q axis.

The frequency contours are plotted in Fig. 3. The Bragg frequencies $\pm\omega_B$ define the points $(p,q) = (\pm k_o, 0)$ where one of the two interacting ocean wavenumbers is zero (i.e., infinite wavelength). Obviously such ocean waves do not exist, and the corresponding directional spectral value in (4) will be zero, together with the value of the second-order radar cross section. This is the reason for the nulls between the first and second-order spectra that can be seen in fig. 1. Close to the Bragg frequency, the frequency contours are almost circular in shape, and have a radius much smaller than the radar wavenumber $k_o$. Therefore both of the scattering wave vectors $\tilde{k}$ and $\tilde{k}'$ are

almost constant in length around the frequency contour with the longer approximately equal in length to $2k_o$. This provides the basis of a method for the linearization and normalization of equation (4) that will be described in sec. 4. The eccentricity of the contours increases with departure from the Bragg frequency until a caustic occurs when $|\omega| = \sqrt{2}\,\omega_B$. This gives rise to singularities in the radar spectrum at these frequencies.

### 2.3.2 The case $m \neq m'$

Squaring the argument of the delta function now gives

$$\omega^2 = g(k + k' - 2\sqrt{kk'}) \ . \tag{15}$$

If we consider first the half plane of (p,q) space for which $k < k'$, then (15) leads to the inequality

$$\omega^2 < g(k' - k) \ . \tag{16}$$

It can be seen from fig. 2 that the maximum value of $(k' - k)$ equals $2k_o$ and occurs when the vectors lie in opposite directions along the p axis. Therefore from (16)

$$\omega^2 < 2gk_o \ , \tag{17}$$

which defines the region between the Bragg lines:

$$\begin{aligned} 0 < \omega \leq \omega_B \quad &\text{for} \quad m = 1,\ m' = -1 \\ -\omega_B < \omega \leq 0 \quad &\text{for} \quad m = -1,\ m' = 1 \ . \end{aligned} \tag{18}$$

A similar proof applies to the left-half plane with the results

$$\begin{aligned} 0 < \omega \leq \omega_B \quad &\text{for} \quad m = -1,\ m' = 1 \\ -\omega_B < \omega \leq 0 \quad &\text{for} \quad m = 1,\ m' = -1 \ . \end{aligned} \tag{19}$$

Frequency contours are shown in fig. 4. As for the case $m = m'$, they are almost circular close to the Bragg frequency but in this case change shape in a regular fashion with increasing frequency displacement from the Bragg line.

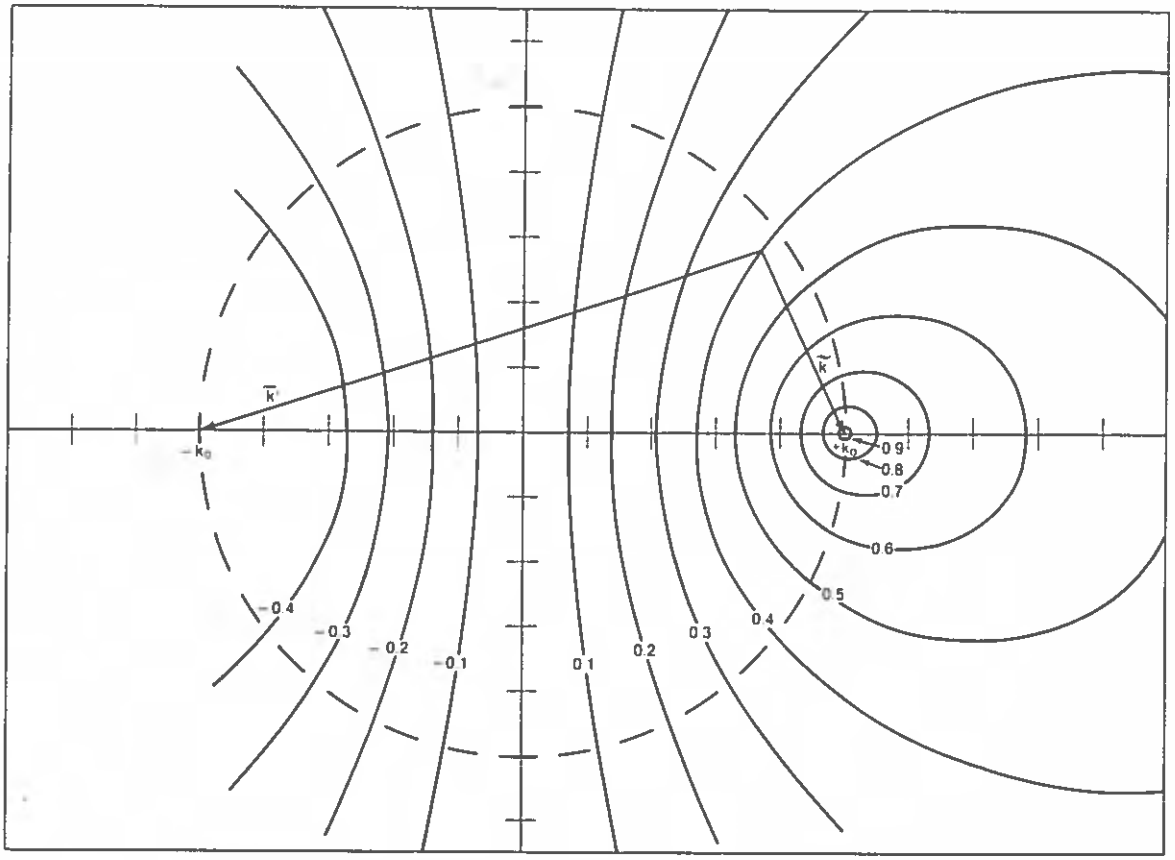


Figure 4.--Normalized constant Doppler frequency contours, $\eta$, vs. wavenumbers k and k', for the two ocean wave vectors $\tilde{k}$ and $\tilde{k}'$ producing second-order backscatter, for $|\omega| < \omega_B$ (i.e., $m = -m'$). The dashed circle representing the electromagnetic 'corner-reflector' condition is not tangent to any Doppler frequency contour; therefore there are no peaks due to this phenomenon between the Bragg lines. The contours are symmetric about the q axis.

# 3. CALCULATION OF THE SECOND-ORDER RADAR CROSS SECTION

In this section, we describe how to calculate values for the second-order radar cross section for a model of the ocean directional waveheight spectrum. It is convenient to transform (4) to a dimensionless form, which is achieved by expressing the product $\omega_B \sigma^{(2)}(\omega)$ as a function of the normalized variables $k/2k_o$ and $\omega/\omega_B$. Results for any calculation then apply to a family of ocean spectral models and radar frequencies having the same values of the normalized parameters. The delta-function constraint is used to perform one of the integrations in (4); the other must generally be performed numerically.

## 3.1 Ocean-Wave Spectral Model

Any model for the ocean-wave spectrum may be used; we choose as an example the product of a Phillips nondirectional equilibrium spectrum and a cardioid directional factor

$$S(\tilde{k}) = f(k)\, g(\theta) \tag{20}$$

where the directional factor is given by

$$g(\theta) = \frac{\cos^s((\theta-\theta^*)/2)}{\int_{-\pi}^{\pi} \cos^s(\theta/2)\, d\theta} \quad . \tag{21}$$

Here s is the so-called ocean-wave spreading factor, and $\theta^*$ is the dominant direction; in certain cases that follow, s and $\theta^*$ will be allowed to vary with wavenumber, k, although in this section we consider them constants, independent of k. The nondirectional spectrum (Phillips, 1977) describes the characteristic falloff of saturated waves above a cutoff wavenumber $k_c$:

$$\begin{aligned} f(k) &= .005/k^4 \quad , \qquad k > k_c \\ f(k) &= 0 \quad , \qquad k \leq k_c \quad . \end{aligned} \tag{22}$$

The wave spectrum is normalized so that the integral over $\tilde{k}$ is equal to the mean square waveheight, $h^2$; i.e.,

$$h^2 = \int_0^{\infty} \int_{-\pi}^{\pi} S(\tilde{k})\, k\, dk\, d\theta \quad . \tag{23}$$

## 3.2 Expression of the Integral in Dimensionless Form

We define the following dimensionless variables:

Wave vector: $\tilde{K} = \tilde{k}/2k_o, \quad \tilde{K}' = \tilde{k}'/2k_o$ (24)

Wavenumber: $K = |\tilde{K}|, \quad K' = |\tilde{K}'|$ (25)

Frequency: $\eta = \omega/\omega_B$ (26)

RMS waveheight: $H = 2k_o h$ (27)

Coupling coefficient: $\gamma_H = \frac{\Gamma_H}{2k_o}$ , $\gamma_{EM} = \frac{\Gamma_{EM}}{2k_o}$ , $\gamma_L = \gamma_H + \gamma_{EM}$ (28)

Nondirectional spectrum: $F(K) = (2k_o)^4 f(k)$ (29)

Ocean-wave directional spectrum: $Z(\tilde{K}) = (2k_o)^4 S(\tilde{k})$, with $K_c = k_c/2k_o$ . (30)

Note that with these definitions, the integral over $Z(\tilde{K})$ is equal to the normalized mean-square waveheight $H^2$. It is also convenient to define through the following equations two new parameters: a dimensionless variable u, which is the magnitude of the normalized frequency shift from the Bragg line,

$$u = m(\eta - m') \ , \tag{31}$$

and a parameter L, which is +1 outside the Bragg lines (where $m = m'$) and -1 within (where $m \neq m'$):

$$L = mm' \ . \tag{32}$$

Using the symmetry condition to be discussed below, the indices m,m' define the four second-order regions of the Doppler spectrum: (i) $m = m' = +1$ corresponds to $\eta > 1$ or $\omega > \omega_B$; (ii) $m = -1$, $m' = +1$ corresponds to $0 < \eta < 1$ or $0 < \omega < \omega_B$; (iii) $m = +1$, $m' = -1$ corresponds to $-1 < \eta < 0$ or $-\omega_B < \omega < 0$; (iv) $m = m' = -1$ corresponds to $\eta < -1$ or $\omega < -\omega_B$. From the definitions (8) and (9) for $\Gamma_H$ and $\Gamma_{EM}$ the normalized coupling coefficients can be written as

$$\gamma_H = \frac{-i}{2}\left[K + K' - \frac{(KK' - \tilde{K}\cdot\tilde{K}')(\eta^2 + 1)}{L\sqrt{KK'}(\eta^2 - 1)}\right] \tag{33}$$

$$\gamma_{EM} = \frac{1}{2}\left[\frac{(K\cdot\hat{k}_o)(K'\cdot\hat{k}_o) - 2\tilde{K}\cdot\tilde{K}'}{\sqrt{\tilde{K}\cdot\tilde{K}'} + \Delta/2}\right] \tag{34}$$

where $\hat{k}_o$ is the unit vector pointing from the radar to the scattering patch. In terms of the dimensionless variables, the delta-function constraint becomes

$$\delta(\omega - m'\sqrt{gk'} - m\sqrt{gk}) = \delta(\eta - m'\sqrt{K'} - m\sqrt{K})/\omega_B \ . \tag{35}$$

By symmetry, the values of the integral in (4) taken over the right and left half planes are identical; we will therefore take the integral only over the right half plane (where $K < K'$) and double the result. We use as integration variables the polar coordinates $K,\theta$ of the shorter scattering wave vector; it can be shown from fig. 2 that in terms of these variables the coordinates of the longer wave vector are

$$K' = \sqrt{K^2 + 2K\cos\theta + 1} \tag{36}$$

$$\theta' = \sin^{-1}(K\sin\theta/K') \ . \tag{37}$$

We can now redefine the first- and second-order radar cross sections (1) and (4) in the following dimensionless form, using equations (24) to (37).

$$\sigma_1(\eta) \equiv \omega_B \sigma^{(1)}(\omega) = 4\pi \sum_{m'=\pm 1} Z(-m'\hat{k}_o)\ \delta(\eta - m'\sqrt{K'}) \tag{38}$$

$$\sigma_2(\eta) \equiv \omega_B \sigma^{(2)}(\omega)$$

$$= 8\pi \sum_{m,m'=1} \int_0^\infty \int_{-\pi}^{\pi} |\gamma_L|^2\ \delta(\eta - m\sqrt{K} - m'\sqrt{K'})\ Z(m\tilde{K})\ Z(m'\tilde{K}')KdKd\theta. \tag{39}$$

## 3.3 Reduction to a Single Integral

One of the integrations in (39) is easily performed using the delta function constraint on the variables. The form of (39) suggests the definition of new variables as follows:

$$y = \sqrt{K} \tag{40}$$

$$h(y,\theta) = my + m'\sqrt{K'} \tag{41}$$

$$I(y,\theta) = 2^4\pi|\gamma_L|^2\ Z(m\tilde{K})\ Z(m\tilde{K}')y^3 \ . \tag{42}$$

Substituting these definitions in (39) gives the following simple form:

$$\sigma_2(\eta) = \iint I(y,\theta)\ \delta(\eta - h(y,\theta))\ dyd\theta$$

$$= \iint I(y,\theta)\ \delta(\eta - h(y,\theta))\ \left|\frac{\partial y}{\partial h}\right|_\theta\ dhd\theta \tag{43}$$

where the factor $\left|\frac{\partial y}{\partial h}\right|_\theta$ can be obtained by differentiating (41).

$$\left|\frac{\partial y}{\partial h}\right|_\theta = \frac{1}{\left|1 + Ly(y^2 + \cos\theta)/(1 + 2y^2\cos\theta + y^4)^{3/4}\right|} \quad . \tag{44}$$

This factor has an integrable singularity at the origin where $\theta = \pi$ and $y = 1/\sqrt{2}$, and at $|\eta| = \sqrt{2}$ (see fig. 3).

In the next section, we show how to solve the delta-function constraint to give y as a function of $\eta$ and $\theta$. Writing this solution as $y^*$, (43) reduces to a single-dimensional integral over angle

$$\sigma_2(\eta) = \int_{-\pi}^{\pi} I(y^*, \theta) \left|\frac{\partial y}{\partial h}\right|_\theta \Bigg|_{y=y^*} d\theta \quad . \tag{45}$$

The integral in (45) cannot in general be solved in closed form. We describe its numerical solution in the remainder of this section.

## 3.4 Solution of the Delta-Function Constraint

We require the solution of the equation

$$\eta - h(y^*, \theta) = 0 \quad . \tag{46}$$

Equation (46) may be solved numerically using a Newton-Raphson method. Defining a function f(y) at fixed $\eta$ and $\theta$ such that

$$f(y) = \eta - h(y, \theta) = \eta - my - m'(1 + 2y^2\cos\theta + y^4)^{1/4} \quad , \tag{47}$$

we may write (46) as

$$f(y^*) = 0 \quad . \tag{48}$$

Expanding (47) about $y^*$ gives

$$f(y) = (y - y^*)\left(\frac{\partial f}{\partial y}\right)_{y=y^*} \quad . \tag{49}$$

According to the Newton-Raphson method, one makes an initial guess at $y_i^*$ and obtains a better approximation $y_{i+1}^*$ from (49):

$$y_{i+1}^* = y_i^* - \left[\frac{f(y)}{(\partial f/\partial y)}\right]_{y=y_i^*} \quad . \tag{50}$$

This process is repeated until the required degree of convergence is attained.

To obtain an initial guess for the iteration, we use the following procedure. Equation (48) may be solved exactly for all frequencies at $\theta = 0,\pi$ for $L = +1,-1$ respectively. The two solutions are given by

$$\begin{aligned} y^* &= (u^2 + 2u)/2(u+1) \quad \text{for} \quad L = 1,\ \theta = 0\ ; \\ y^* &= (u - 1 + \sqrt{1 + 2u - u^2})/2 \quad \text{for } L = -1,\ \theta = \pi\ ; \end{aligned} \tag{51}$$

where u is defined in (31). We therefore start the numerical integration of (45) over angle at these values. The initial guess at successive values of $\theta$ around the frequency contour is taken to be the solution of (48) at the preceding quadrature point.

Close to the Bragg lines, a simpler method is available. When $y \ll 1$, the solution to (48) can be written to first order in a form that is independent of angle (corresponding to almost circular frequency contours):

$$y^* \approx m(\eta - m') = u \quad . \tag{52}$$

This result may be used as an initial guess throughout the numerical integration.

## 3.5 Calculation of the Coupling Coefficient

Program 1 (Appendix B) calculates the normalized coupling coefficient from eqs. (33) and (34) for input values of K and $\theta$. The quantity calculated is the total coupling coefficient $|\gamma_L|^2$, where $\gamma_L$ is defined in (28). The calculation is performed in terms of the variable y defined in (40) and uses the following substitutions

$$\tilde{K}\cdot\tilde{K}' = \tilde{K}\cdot(-\hat{k}_o - \tilde{K}) = -K\cos\theta - K^2 \tag{53}$$

$$\frac{\eta^2+1}{\eta^2-1} = \frac{(\sqrt{K}+L\sqrt{K'})^2+1}{(\sqrt{K}+L\sqrt{K'})^2-1} \quad . \tag{54}$$

The surface impedance $\Delta$ is slightly dependent on the directional ocean-wave spectrum; however the value of the coupling coefficient is insensitive to the value of $\Delta$ except when the scalar product $K\cdot K'$ in the denominator of (34) approaches zero. This produces a singularity in the electromagnetic coupling coefficient and marks the transition between propagating and evanescent intermediate radio waves scattered between the two ocean wavetrains. The condition $K\cdot K' = 0$ defines a circle in the (p,q) plane, which is shown in figs. 3 and 4. The effect of the singularity on the value of the radar cross section is small except for normalized frequencies close to $2^{3/4}$. At this point, the frequency contour becomes tangential to the circle of singularity. In our work to date with long ocean waves, frequencies in this region have not been of importance, since the contributing ocean waves at the $2^{3/4}$ singularity have short periods approximately $2^{1/4}$ times the period of the first-order Bragg waves. We have therefore found it adequate to use the following constant value for $\Delta$ over the HF region:

$$\Delta = .011 - i(.012) \quad . \tag{55}$$

This assumption must be reevaluated if one is interested in shorter-period waves (i.e., less than twice the period of the Bragg waves).

We include a sample output from Program 1 (Appendix B), for input values of $K = 0.05$ and values of $\theta$ in steps of 10° from 0° to 180°.

## 3.6 Integration Limits

It can be seen from figs. 3 and 4 that for integration over the right-half plane, the value of $\theta$ defined by a frequency contour usually ranges from $-\pi$ to $\pi$. However for $\eta^2 > 2$, the contour intersects the q axis, and the

limits on $\theta$ must be obtained by solving for the points of intersection. It follows from fig. 2 that at the q axis, where K and K' are equal, the limiting values $\theta_L$ are given by

$$\theta_L = \pm [\pi - \cos^{-1}(2/\eta^2)] \text{ for } \eta^2 > 2 . \quad (56)$$

## 3.7 Numerical Computation of the Sea-Echo Doppler Spectrum

Program 2 (Appendix C) calculates the normalized second-order radar cross section for the ocean-wave spectral model described in sec. 3.1. We have found that it is normally adequate to use 36 quadrature points for the integration over angle (that is, at least one point every 10°). There is provision in the program to increase the number of quadrature points in the neighborhood of the $2^{3/4}$ singularity. Spectral points near zero Doppler are not calculated; they have been of little interest to us because they are produced by short ocean waves (with periods less than $\sqrt{2}$ times the Bragg-wave period), and the calculation must be modified as the frequency contour becomes infinitely long. Numerical output from Program 2 is included for the following input parameters: $K_C = .03$, $\theta^* = 45°$, $s = 4$, and for normalized frequencies in the range $-2$ to $+2$.

Figures 5 and 6 give examples of simulated spectra calculated from (38) and (39). To simulate the finite frequency resolution of a practical system, we have smeared the theoretical Doppler spectrum in normalized frequency using a Gaussian window of width 0.1. Figure 5 illustrates the effect of changing waveheight; the Doppler spectrum is shown for three different values of waveheight at the same dominant ocean-wave direction (135° with respect to the radar beam). For the ocean-wave spectral model used, increasing waveheight is equivalent to increasing the peak waveperiod. The resulting amplitude of the second-order spectrum increases relative to the first, and the spectral peak moves closer to the Bragg line. Figure 6 illustrates the effect of changing the dominant wave direction at constant waveheight; the Doppler spectrum is shown for three values of dominant wave direction, $\theta^*$, relative to the radar beam (180°, 135°, 90°). The degree of symmetry about zero Doppler increases as the wave direction tends to perpendicular.

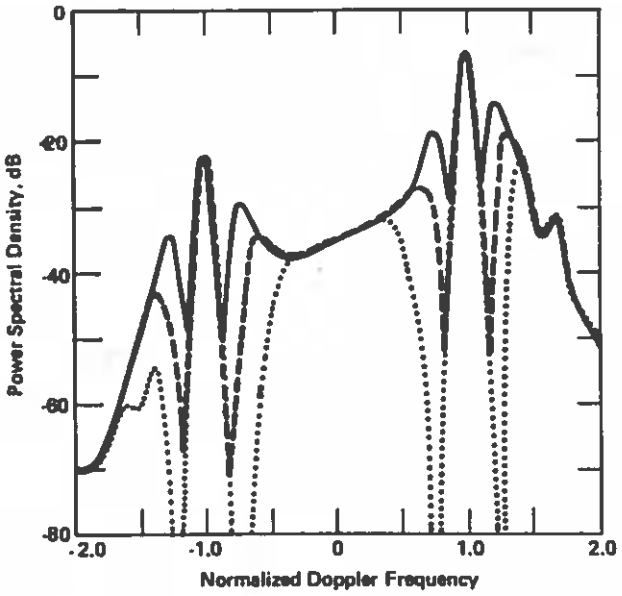


Figure 5.--Simulated spectra showing the effect of increasing wave-height on the normalized radar Doppler spectrum defined by (38) and (39). We have used the cardioid model defined by (20) for the directional ocean wave-height spectrum with ocean-wave direction equal to 135° with respect to the radar beam and normalized wave-heights of 1.0 (continuous line), 0.5 (dashed), and 0.2 (dotted). The whole spectrum is smeared in normalized frequency using a Gaussian window of width 0.1.

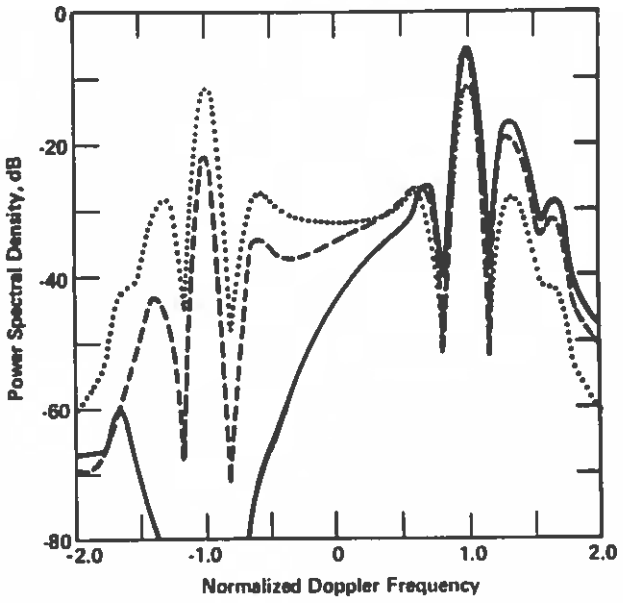


Figure 6.--Simulated spectra showing the effect of changing ocean-wave direction (relative to the radar beam) on the normalized radar Doppler spectrum. The ocean-wave spectral model and the frequency smearing are the same as for fig. 5; the normalized waveheight is equal to 0.5, and the ocean-wave directions are 180° (continuous line, 135° (dashed), and 90° (dotted).

# 4. INVERSION FOR LONG-PERIOD OCEAN-WAVE PARAMETERS

From the theoretical radar spectra shown in figs. 5 and 6, it is clear that the spectral shape is sensitive to changing ocean-wave conditions. In this section, we will show how to estimate long-period ocean-wave parameters from the radar data. These methods require a linearization of the integral equation (4) for the second-order radar cross section; we restrict consideration to the long-period region because our linearization method (to be described in sec. 4.2) applies there. Estimation of short-period wave parameters requires solution of the nonlinear problem and will not be discussed here.

## 4.1 Initial Data Treatment

To reduce the statistical variance, we must average spectra from different range cells and time periods and produce a composite spectrum to be analyzed. Barrick and Snider (1977) have shown that the sea-echo power spectrum after N-sample averaging is $\chi^2$ distributed with 2N degrees of freedom. They also show that Doppler spectra (both first and second order) become uncorrelated for time intervals greater than approximately 25 s for radar frequencies greater than 10 MHz, and that Doppler spectra from different range cells are statistically independent. These experimental results may be used to optimize the amount of incoherent averaging. Statistical accuracy may also be increased by averaging adjacent frequency points, at the expense of spectral frequency resolution. In practice, about 100 spectra should be incoherently averaged, if possible, before analysis. Before averaging, individual power spectra should be normalized in amplitude to increase the number of degrees of freedom in the composite spectrum if different unknown path losses are suspected of multiplying the individual spectra (e.g., as with skywave radar data, or groundwave data from different ranges). The simplest method is to divide the total spectrum by the energy contained in the dominant Bragg line. Barrick (1980) analyzes the error propagation in this process.

Before analyzing the composite spectrum for ocean-wave parameters, we must remove the frequency bias produced by ocean surface currents and/or ionospheric motion. We first find the centroid frequencies, $\omega_c^{\pm}$, of the first order regions that are bounded by the frequency nulls (see fig. 1), using the formula

$$\omega_c = \sum_i \sigma^{(1)}(\omega_i)\ \omega_i / \sum_i \sigma^{(1)}(\omega_i) \quad . \tag{57}$$

The average bias estimate to be subtracted from all frequencies is given by

$$\Delta\omega = \frac{(\omega_c^{+} + \omega_c^{-})}{2} \quad . \tag{58}$$

## 4.2 Linearization of the Integral Equation

To simplify the integral equation, we use a linearization scheme proposed by Barrick (1977). We have already noted in sec. 2.3, with reference to the frequency contours shown in figs. 3 and 4, that for frequencies close to the Bragg line, the wave vector of the shorter scattering ocean wave is approximately equal to the Bragg wave vector, i.e.,

$$\tilde{K}' \approx -2\hat{k}_o \quad . \tag{59}$$

The directional spectral factor in the integrand at this wave vector is therefore approximately equal to that for the Bragg wave, which can be obtained from the neighboring first-order line. These waves normally lie in the saturated region of the ocean-wave spectrum. However, a better approximation is obtained by including the wavenumber variation along the constant-Doppler contour, assuming the Phillips equilibrium spectrum:

$$Z(m'\tilde{K}') = \frac{Z(-m'\hat{k}_o)}{K'^4} \quad . \tag{60}$$

Substituting this expression into (39) and normalizing by the energy in the neighboring first-order line gives the following expression for the energy ratios:

$$R_{m,m'}(u) = \frac{\mathcal{Z}(\eta)}{\int \sigma_1(\eta)\,d\eta}$$

$$= 2 \int_0^{\infty} \int_{-\theta_L}^{\theta_L} |\gamma_L|^2 \, \delta(mu+m'-m\sqrt{K}-m'\sqrt{K'}) \, Z(m\tilde{K}) \, \frac{K}{K'^4} \, dK d\theta \tag{61}$$

where u is the normalized frequency displacement from the Bragg positions at $m' = \pm 1$, defined in terms of $\eta$ by (31) for any given sideband. (The limits $\theta_L$ were defined and discussed in sec. 3.6.)

We define the following notation convention for use throughout this section: Uppercase R's denote theoretical quantities, whereas lower-case r's are measured quantities; script $\mathcal{R}$'s denote the total energy in the peak, whereas block R's denote the actual peak function.

The above, (61), actually represents four equations, one corresponding to each of the four second-order sidebands surrounding the two first-order Bragg lines. These four, as before, are defined by $m,m' = \pm 1$; i.e., $m' = \pm 1$ defines the positive/negative Doppler spectral lines, and $m = \pm 1$ locates the second-order peak as being either to the right/left of the surrounded Bragg line (see fig. 1). This expression (61) is a linear integral equation for the waveheight directional spectrum. In addition, unknown calibration factors and path losses have been removed from the data by normalization of one portion of the spectrum by another.

This linearization method applies for long ocean waves such that the normalized wavenumber K is less than 0.06; the corresponding value of the frequency shift u is less than 0.25. For example, for a 25-MHz radar transmitter frequency, it is valid for ocean-wave periods longer than about 8 s.

## 4.3 The 'Bands' Approximation

As we have shown in sec. 2.3, the frequency contours in figs. 3 and 4 are approximately circular close to the Bragg frequency. Thus a given Doppler shift corresponds to a narrow band of ocean wavenumbers, the approximate relationship between wavenumber K and wave direction $\theta$ being given by

$$u \approx \sqrt{K}\ (1 + \frac{L}{2}\sqrt{K}\cos\theta)\ . \qquad (62)$$

In a single Doppler spectrum there are therefore four independent pieces of information (corresponding to the four sidebands) on the ocean-wave spectrum at any wavenumber. This results in considerable simplification of the inverse problem.

The width of the wavenumber band vs. $\theta$ corresponding to a given Doppler shift is least when very close to the Bragg frequency. Further removed, the width increases, resulting in a frequency smearing of the derived ocean-wave spectrum. To derive the width of the band, note from fig. 3 that for $m = m'$, the maximum and minimum values of wavenumber ($K_u$ and $K_L$) on a frequency contour occur at $\theta = 180°, 0°$, respectively. They can therefore be obtained from the exact equations

$$u = \sqrt{K_u} + \sqrt{1 - K_u} - 1 = \sqrt{K_L} + \sqrt{1 + K_L} - 1 \ . \tag{63}$$

For small values of u and K the solutions to these equations are

$$K_u \approx u^2 + u^3 \quad ; \quad K_L \approx u^2 - u^3 \ . \tag{64}$$

For $m \neq m'$, the maximum and minimum values of normalized wavenumber occur at $\theta = 0°, 180°$, respectively, and can be obtained from the equations

$$u = \sqrt{K_L} - \sqrt{1 - K_L} + 1 = \sqrt{K_u} - \sqrt{1 + K_u} + 1 \ , \tag{65}$$

which have exactly the same solutions (64) as the case $m = m'$, for small values of K and u. The maximum wavenumber excursion corresponding to a given frequency shift u is therefore approximately given by

$$\Delta K = 2u^3 \ . \tag{66}$$

## 4.4 Limitations of the Information From Narrow-Beam Radars

### 4.4.1 Single narrow beam

Here we show that the amount of waveheight directional spectral information obtainable from a single narrow-beam look at a patch of ocean is quite limited. This is most easily illustrated by expanding the normalized directional spectrum in a Fourier series vs. angle:

$$Z(m\tilde{K}) = \frac{1}{2\pi} \sum_{n=-N}^{N} c_n(K)\ m^n\ tf_n(\theta) \ , \tag{67}$$

where the coefficients $c_n$ are functions of normalized wavenumber and the trigonometric functions $tf_n$ are defined by

$$tf_n(\theta) = \begin{cases} \cos(n\theta) & n \geq 0 \\ \sin(|n|\theta) & n < 0 \ . \end{cases} \tag{68}$$

As in sec. 3, we use the delta function constraint to perform one of the integrations in (61), giving

$$R_{m,m'}(u) = 4 \int_{-\pi}^{\pi} |\gamma_L|^2 \, y^3 \left|\frac{\partial y}{\partial h}\right|_\theta Z(m\tilde{K}) \, \frac{d\theta}{K'^4} \quad , \tag{69}$$

where $\left|\frac{\partial y}{\partial h}\right|_\theta$ is given by (44). At this point, we plan to expand everything except $Z(m\tilde{K})$ in the integrand of (69) in terms of u, retaining only terms up to first order, using

$$\sqrt{K} = y = u - \frac{L}{2} u^3 \cos\theta \ . \tag{70}$$

To first order in u, we note that a good approximation to $|\gamma_L|^2$ (Lipa and Barrick, 1980) is:

$$|\gamma_L|^2 = \begin{cases} \frac{1}{4}\cos^2\theta(1 - 2u) & \text{for} \quad -\frac{\pi}{2} \leq \theta \leq \frac{\pi}{2} \\ \frac{1}{4}\cos^2\theta & \text{for} \quad \frac{\pi}{2} \leq \theta \leq \frac{3\pi}{2} \ . \end{cases} \tag{71}$$

Likewise, to the same order in u, we find

$$y^3 \left|\frac{\partial y}{\partial h}\right|_\theta = u^3(1 - \frac{5}{2} L \, u \cos\theta) \ . \tag{72}$$

If we now substitute these into (69) we obtain

$$R_{m,m'}(u) = \sum_{n=-N}^{N} c_n(K) \, a_n \ , \tag{73}$$

where

$$a_n = \frac{u^3}{2\pi}\left\{ \int_{-\pi/2}^{\pi/2} [1 - u(2 + \frac{5}{2}\cos\theta)] \cos^2\theta \, m^n \, tf_n(\theta) \, d\theta \right.$$

$$\left. + \int_{\pi/2}^{3\pi/2} [1 - \frac{5}{2}\cos\theta] \cos^2\theta \, m^n \, tf_n(\theta) \, d\theta \right\} . \tag{74}$$

For values of u less than 0.25, we therefore obtain the following solutions for the four sidebands

m = 1, m' = 1:

$$a_o = u^3(1-u)/2; \quad a_1 = -u^4(5/4+4/3); \quad a_2 = u^3(1-u)/4; \quad a_{-1}=a_{-2}=\ldots=a_{-n}=0 .$$

m = -1, m' = 1:

$$a_o = u^3(1-u)/2; \quad a_1 = -u^4(5/4-4/3\pi); \quad a_2 = u^3(1-u)/4; \quad a_{-1}=a_{-2}=\ldots=a_{-n}=0 .$$

m = 1, m' = -1:

$$a_o = u^3(1-u)/2; \quad a_1 = +u^4(5/4-4/3\pi); \quad a_2 = u^3(1-u)/4; \quad a_{-1}=a_{-2}=\ldots=a_{-n}=0 .$$

m = -1, m' = -1:

$$a_o = u^3(1-u)/2; \quad a_1 = +u^4(5/4+4/3\pi); \quad a_2 = u^3(1-u)/4; \quad a_{-1}=a_{-2}=\ldots=a_{-n}=0 .$$

We can draw the following conclusions from these results:

(1) Since $a_{-1} = 0$, none of the odd Fourier coefficients multiplying the sine functions are determinable from a single narrow-beam look. The meaning of this, which is obvious physically, is that there is a right/left ambiguity about the radar beam; it is therefore impossible to tell from which side the waves are coming. Independent information must be used if this ambiguity is to be resolved.

(2) For all four sidebands, we note that $a_2 = a_o/2$; this is true only to the order in u to which we have carried our approximation. If we define the directional spectrum by five Fourier coefficients (i.e., N = 2 in (67)), the four sideband amplitudes at a given value of u are therefore functions of two factors only:

$$c_1(K), \quad c_o(K) + c_2(K)/2 \tag{75}$$

where, from (62), K is approximately equal to $u^2$. It follows that it will be impossible to separate $c_o(K)$ and $c_2(K)$ from the data, to order u in our series. To order $u^2$ they are separable, but since u is a small number, statistical fluctuations in the data will cause large uncertainties in $c_o(K)$ and $c_2(K)$ if one forces their separation. Sometimes accuracy can be increased by

using other information derived from the frequency centroids of the four sidebands, as described in sec. 4.5.

(3) Large statistical uncertainties can also be expected in parameters derived by fitting cardioid models of the ocean-wave spectrum to the radar data. Rewriting (20) for the cardioid model in normalized form gives

$$Z(\tilde{K}) = \frac{F(K)\ \cos^{s}\left(\frac{\theta-\theta^{*}}{2}\right)}{\int_{-\pi}^{\pi} \cos^{s}(\theta/2)\ d\theta} \quad . \tag{76}$$

The Fourier coefficients $c_n$ have the following relationship to the parameters of (76) (Barrick and Lipa, 1979)

$$\begin{aligned} c_o(K) &= F(K) \\ c_1(K) &= \frac{2s}{(s+2)} \cos\theta^{*}\ F(K) \\ c_2(K) &= \frac{2s\,(s-2)}{(s+2)(s+4)} \cos 2\theta^{*}\ F(K) \quad . \end{aligned} \tag{77}$$

These equations show that, since it is difficult to separate $c_o(K)$ and $c_2(K)$ from the data, the three parameters $F(K)$, $s$, and $\theta^{*}$ will also have large statistical uncertainties; examples illustrating these large uncertainties will be examined later.

### 4.4.2 Two narrow beams

To study the quality of information obtainable from two radar beams inclined at an angle $\varepsilon$, we define two sets of Fourier coefficients $c_i(K)$ and $c_i^{(2)}(K)$ with reference to the first and second beams. From the definition (67), we can write the following equations for the directional ocean-wave spectrum at an arbitrary angle $\varepsilon$ with respect to the second beam:

$$Z(m\tilde{K}) = \frac{1}{2\pi} \sum_{n=-N}^{N} c_n^{(2)}(K)\ tf_n(\theta) = \frac{1}{2\pi} \sum_{n=-N}^{N} c_n(K)\ m^n\ tf_n(\theta+\varepsilon) \ , \tag{78}$$

leading to the following identities:

$$c_o^{(2)}(K) = c_o(K)$$

$$c_1^{(2)}(K) = c_{-1}(K)\ \sin\varepsilon + c_1(K)\ \cos\varepsilon \qquad (79)$$

$$c_2^{(2)}(K) = c_{-2}(K)\ \sin 2\varepsilon + c_2(K)\ \cos 2\varepsilon\ .$$

To first order in u, therefore, the following pieces of independent information are available from two narrow beams:

$$c_1(K),\ c_o(K) + \frac{c_2(K)}{2}\ ,\ c_{-1}(K)\ \sin\varepsilon + c_1(K)\ \cos\varepsilon,\ \text{and}$$
$$c_o(K) + \frac{c_{-2}(K)}{2}\ \sin 2\varepsilon + \frac{c_2(K)}{2}\ \cos 2\varepsilon\ . \qquad (80)$$

By substitution of the relations (77) for the cardioid model parameters, (80) becomes

$$\frac{2s\ \cos\theta^*\ c_o(K)}{(s+2)}\ ,\quad c_o(K)\left(1 + \frac{s(s-2)\cos 2\theta^*}{(s+2)(s+4)}\right)\ ,\quad c_o(K)\left(\frac{2s}{s+2}\cos(\theta^* - \varepsilon)\right)\ ,\ \text{and}$$
$$c_o(K)\left(\frac{s(s-2)\ \cos 2(\theta^* - \varepsilon)}{(s+2)(s+4)}\right)\ . \qquad (81)$$

Although one cannot hope to derive five Fourier coefficients using (80) from the four pieces of information, it is apparent from (81) that a stable determination of the three parameters $s, \theta^*$, and $c_o(K)$ (the first two also being functions of wavenumber, K) should be possible.

These approximate conclusions will be verified in sec. 4.5, where we estimate the statistical uncertainties in least-squares fitting procedures for both single and double narrow-beam observations.

## 4.5 Interpretation Yielding Ocean-Wave Parameters at a Single Dominant Wavenumber

When the widths of the first- and second-order spectral peaks are comparable (as in fig. 1), we can interpret the Doppler spectrum in terms of an ocean-wave spectral model with a single dominant wavenumber and a cardioid directional distribution

$$S(\tilde{k}) = \frac{h^2 \cos^s\left(\frac{\theta-\theta^*}{2}\right) \delta(k-k^*)}{k \int_{-\pi}^{\pi} \cos^s(\theta/2)\, d\theta} \tag{82}$$

where h is the RMS waveheight, $k^*$ and $\theta^*$ are the dominant wavenumber and direction, and s is the spreading factor.

In the normalized form described in sec. 3.2, (82) becomes

$$Z(\tilde{K}) = \frac{H^2 \cos^s\left(\frac{\theta-\theta^*}{2}\right) \delta(K-K^*)}{K \int_{-\pi}^{\pi} \cos^s(\theta/2)\, d\theta} \quad . \tag{83}$$

### 4.5.1 Single narrow beam

#### *Second-order peak frequencies*

For such ocean-wave spectra, the Doppler spectrum has four reasonably sharp distinguishable sidebands. We may define the second-order sideband frequencies by setting the argument of the delta-function constraint in (39) equal to zero, giving for a single radar beam

$$\eta_{m,m'} = m\ K^* + m'(1 + 2mK^* \cos\theta^* + K^{*2})^{1/2} \quad . \tag{84}$$

This definition is exact only when the wave spectrum becomes infinitesimally narrow in angle (i.e., $s \to \infty$). Lipa and Barrick (1980) and Lipa et al. (1981) find, however, that this definition gives a quite adequate description of the sideband frequency centroids even for s as low as 2.

The optimum choice for the parameters $K^*$ and $\theta^*$ can be obtained from (84) by employing the least-squares fitting methods described in Appendix A. However, it is often more convenient to use closed-form solutions that follow from (84):

$$K^* = (\Delta\eta^+ + \Delta\eta^-)^2/16 \tag{85}$$

$$\theta^* = \cos^{-1}\left(\frac{8(\Delta\eta^+ - \Delta\eta^-)}{(\Delta\eta^+ + \Delta\eta^-)^2}\right) \tag{86}$$

where $\Delta\eta^+$ and $\Delta\eta^-$ are the frequency displacements between the sidebands surrounding the positive and negative Bragg lines (see fig. 1).

The values of $\eta_{m,m'}$ are calculated by finding the centroid frequency of the spectral peak between the half-power points. Barrick (1980) has calculated a general expression for the standard deviation of a centroid frequency for a power spectrum that obeys $\chi^2$ statistics. This expression is insensitive to the exact shape of the peak; therefore Barrick shows that if we assume a Gaussian form for convenience, the standard deviation of the frequency estimate is

$$Sd(\omega) = \frac{\Delta}{2}(M/N)^{1/2} \tag{87}$$

where M is the number of samples contained within the half-power width, N is the number of independent spectra used in the sample average, but here $\Delta$ is the angular frequency spacing between adjacent spectral points. The corresponding uncertainties in the estimates (85) and (86) for $K^*$ and $\theta^*$ follow from linear error propagation theory (Brandt, 1970)

$$Sd(K^*) = \frac{\Delta}{2}\left(\frac{K^* M}{N}\right)^{1/2} \tag{88}$$

$$Sd(\theta^*) = 8\Delta(M/N)^{1/2}\left|\frac{[5(\Delta\eta^+)^2 - 6\Delta\eta^+\Delta\eta^- + 5(\Delta\eta^-)^2]^{1/2}}{\sin\theta^*(\Delta\eta^+ + \Delta\eta^-)^3}\right| \quad \text{for } \sin\theta^* \neq 0 \text{ .} \tag{89}$$

The uncertainty in the estimate of wavenumber is generally small; that in angle can be large because of the differencing of small frequency shifts in (86).

## *Second-order peak energy ratios*

Substitution of the spectral model (83) into the linearized equation (61) gives the following model for the ratio between the second-order peak energy and the energy in the neighboring first-order line:

$$R_{m,m'} = H^2 \Phi_{m,m'}(\theta^*, \Delta\theta^*) \tag{90}$$

where

$$\Phi_{m,m'}(\theta^*, \Delta\theta^*) = \frac{2}{\int_{-\pi}^{\pi} \cos^s(\theta/2)d\theta} \int_{-\pi}^{\pi} \left|\gamma_L\right|^2_{K^*,\theta} \cos^s\left(\frac{\theta-\theta^* + (m-1)\pi}{2}\right)\frac{d\theta}{K'4} \quad . \tag{91}$$

The factor (91) is calculated at the value of $K^*$ obtained from the sideband frequencies, through (85). The spreading factor s in the above equation is related to the half-power beamwidth $\Delta\theta^*$ by the equation (Barrick and Lipa, 1979)

$$s = \frac{\ell n(0.5)}{\ell n[\cos(\Delta\theta^*/4)]} \quad . \tag{92}$$

We use the least-squares method to fit the theoretical expression to the data. In this method, described in Appendix A, we minimize the sum of weighted squared deviations of the data from the ideal functional forms to give the optimal parameters. The quantity to be minimized is

$$I = \sum_{m,m'} \frac{(\mathcal{R}_{m,m'} - R_{m,m'})^2}{(\Delta\mathcal{R}^2_{m,m'})} \quad , \tag{93}$$

where $\mathcal{R}_{m,m'}$ are the normalized energies of the measured second-order peaks defined in (61). We note that $\mathcal{R}_{m,m'}$ is the ratio of sums of $\chi^2$ power spectral samples and is therefore itself a random variable that follows an F distribution (Barrick, 1980). If the numerator and denominator are sums of $N_1$ and $N_2$ independent power samples, respectively, in the limit of large $N_2$ (i.e., $N_2 \geq 5$), the F distribution becomes $\chi^2$ with an effective number of spectral averages $N_e$ given by

$$1/N_e = 1/N_1 + 1/N_2 \quad . \tag{94}$$

The variance in the denominator of (93) is therefore given by:

$$\Delta^2 \mathcal{R}_{m,m'} = \frac{\mathcal{R}^2_{m,m'}}{N_e} \quad . \tag{95}$$

To calculate $N_e$, we require the equivalent number of spectral samples ($N_1$, $N_2$) in the calculation of the first- and second-order peak energies. According to Barrick (1980) these are approximately given by

$$N_i = 1.3\ NM\ , \tag{96}$$

where N and M are defined following (87).

Program 3 (Appendix D) calculates the elements $\Phi_{m,m'}(\theta^*, \Delta\theta^*)$ for a range of parameter values; a sample output is included. Using these elements, we can simply perform a grid search over parameter space to find the minimum value of I ($I_{min}$). I and $I_{min}$ are $\chi^2$ distributed† with 4 and 4-n degrees of freedom, where n is the number of parameters fit to the data. The parameters defining $I_{min}$ are then the optimum choice. As described in Appendix A, to set confidence limits on the derived parameters, we calculate the following statistic throughout parameter space:

$$Z = (I - I_{min})/I_{min}\ . \tag{97}$$

Z is distributed as $\frac{n}{(4-n)} F(n, 4-n)$, and tables of the F distribution may be used to define confidence contours. This process is illustrated later in this section by application to simulated data.

We leave as an open question for now how many parameters, n, are to be fitted to the data in the least-squares manner described in this subsection. For example, if both $K^*$ and $\theta^*$ can be determined accurately using the peak frequencies method described after (84), then only $\Delta\theta^*$ and $H^2$ are unknown, and n = 2. On the other hand, it is often possible to determine only $K^*$ accurately from the peak frequencies; then $\theta^*$, $\Delta\theta^*$, and $H^2$ are unknown, and n = 3. This question will be discussed using examples in sec. 4.5.3 below.

---

† We note that both I and the radar power spectrum are $\chi^2$ distributed; the number of degrees of freedom in the two cases is given by the number of equations fitted and the number of spectral averages, respectively.

### 4.5.2 Two narrow beams

We use all the equations in sec. 4.5.1 with reference to Beam 1. There is now a similar set for Beam 2; the angle $\theta$ is replaced by $(\theta-\varepsilon)$, where $\varepsilon$ is the angle between radar beams. Thus the following equation gives the sideband frequencies $\eta^{(2)}_{m,m}$ for Beam 2, corresponding to (84) for Beam 1.

$$\eta^{(2)}_{m,m'} = m\sqrt{K^*} + m'(1 + 2mK^* \cos(\theta^*-\varepsilon) + K^{*2})^{1/4} . \qquad (98)$$

Estimates of $K^*$ and $\theta^*$ can be now obtained from (84) and (98) by minimizing the sum of the squared deviations from the eight observed centroid frequencies.

Similarly, in addition to (90) for the energy ratios of Beam 1, we have the following expression for Beam 2

$$R^{(2)}_{m,m'} = H^2 \Phi_{m,m'}(\theta^*-\varepsilon, \Delta\theta^*) . \qquad (99)$$

Estimates of H and $\theta^*$ can be obtained by least-squares fitting to the eight energy ratios at the value of $K^*$ obtained from the peak frequencies. The sum of squared deviations to be minimized is given by

$$I = \sum_{m,m';i=1,2} \frac{\left(r^{(i)}_{m,m'} - R^{(i)}_{m,m'}\right)^2}{(\Delta r^2_{m,m'})^{(i)}} \qquad (100)$$

where the superscript (i) refers to the beam number. Since we are fitting to eight equations, the statistic Z defined in (97) is distributed as $\frac{n}{(8-n)} F(n, 8-n)$; tabulated values of the F distribution are used to define confidence intervals in parameter space. Again, the question of how many parameters are to be determined using least-squares fitting on (98) vs. least-squares on (99) is left open here; it is considered in the next section.

### 4.5.3 Application to simulated data

To illustrate these statistical techniques, we apply them to simulated data calculated for both single and double narrow-beam systems. To generate the simulated data, energy ratios are calculated from eqs. (90) and (99) with the following parameters: $\varepsilon = 30°$, $s = 4$, $K^* = .05$, $\theta^* = 45°$, RMS waveheight = 0.6 m, radar transmitter frequency = 15 MHz (therefore the corresponding value of H, the normalized waveheight, is 0.38). Thus, the dominant wave direction was taken to be 45° with respect to the first radar beam and 15° with respect to the second. Noise is added randomly to the calculated values consistent with the signal variance defined in (94); 100 effective sample averages are assumed.

#### *Three-parameter fit*

We first attempt to estimate the parameters h, $\theta^*$, and $\Delta\theta^*$ by calculating the sum of squared residuals, I, at each point of a three-dimensional grid in parameter space, using the elements $\Phi_{m,m'}(\theta^*, \Delta\theta^*)$ calculated by Program 3 (Appendix D). We assume $K^*$ was calculated from (85). We chose the following increment sizes: 15° for both direction and beamwidth, 2.5 cm for RMS waveheight.

For a single beam (i.e., the first beam as defined above), the minimum value of I was found to be 3.81. Since we are fitting four equations with three parameters, there is a single degree of freedom. We choose a significance level of 5% and note that $\chi^2_{0.95} = 3.84$. $I_{min}$ is less than this value; we therefore conclude by the $\chi^2$ test that the model fit is satisfactory. In the process of generating $I_{min}$, values for $\mathcal{R}_{m,m'}$ were generated with random noise added to the model in the numerator of (93) such that the numerator variance is close to the variance $\Delta\mathcal{R}^2_{m,m'}$ in the denominator. This is necessary if the simulation is to be reasonable and typical of actual data. Then the value of each term of the least-squares sum will be of the order of unity, as it should.

The statistic Z defined in (97) is distributed as 3F(3,1); the 50% and 75% confidence contours are therefore defined by Z = 5.13 and 24.6, respectively. Figure 7 shows the projection of these contours on the h-$\theta^*$ and h-$\Delta\theta^*$

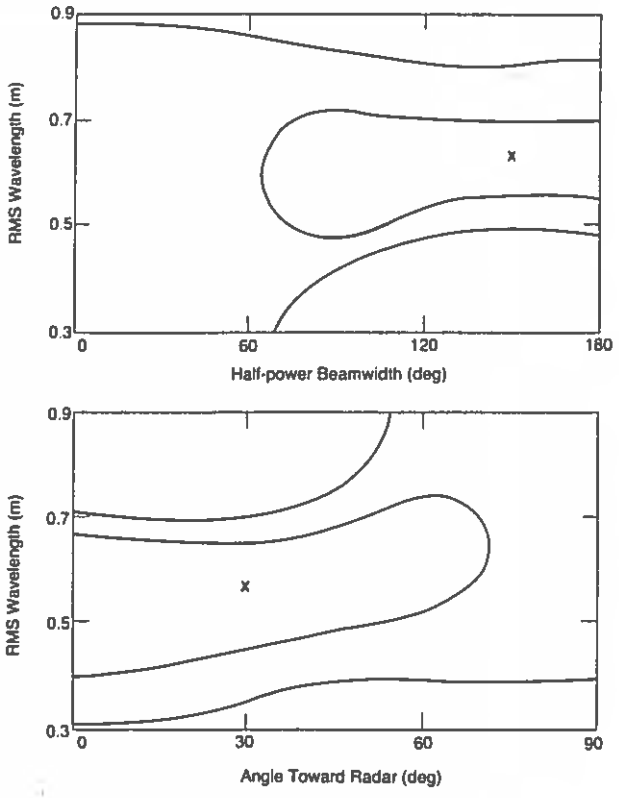


Figure 7.--Confidence contours from the three-parameter maximum-likelihood fit to the energy ratios for a single-beam radar. The x indicates the optimum fit; the outer and inner curves represent the 75% and 50% confidence limits. The upper diagram is the projection of the contours on the h - $\Delta\theta^*$ plane; the lower, on the h - $\theta^*$ plane. Note that $\theta^*$ represents the angle away from the radar, whereas the horizontal axis represents the angle toward the radar (i.e., 180 - $\theta^*$).

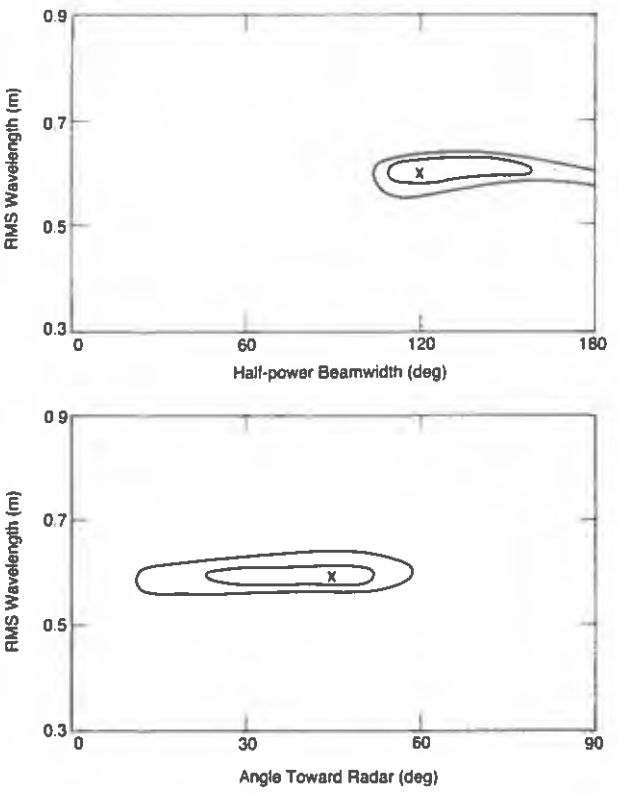


Figure 8.--Confidence contours from the three-parameter maximum-likelihood fit to the energy ratios, as in fig. 7, but for a double-beam system.

planes. It is apparent that fitting three parameters to the power ratios does not provide accurate estimates.

For two beams, $I_{min}$ was found to be 8.2. There are now eight equations fitted by the three parameters and therefore five degrees of freedom. The value of $\chi^2_{0.95}$ is 11.05; since $I_{min}$ is less than this value, the model fit is considered acceptable. The statistic Z is distributed as $\frac{3}{5}F(3,5)$; fig. 8 shows the projection of the 50% and 75% contours on the h-$\theta^*$ and h-$\Delta\theta^*$ planes.

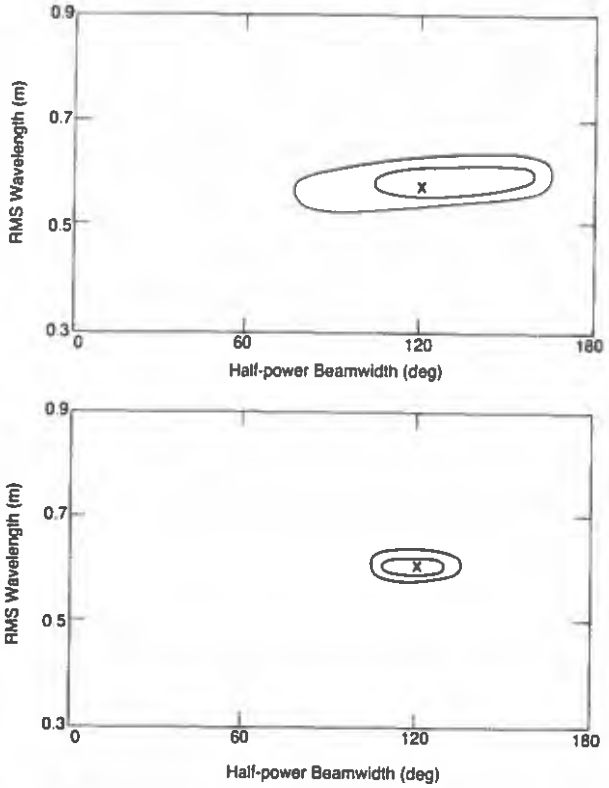


Figure 9.--Confidence contours from the two-parameter maximum-likelihood fit to the energy ratios (outer: 75% confidence; inner: 50%). The upper and lower diagrams are for single- and double-beam systems, respectively.

Clearly, the confidence intervals are far tighter than for the single-beam case, as might have been expected from the discussion of sec. 4.4. At the 75% confidence limit, h, $\theta^*$, and $\Delta\theta^*$ are determined to 7 cm, 45°, and 60°, respectively. Note that this corresponds to 2.4 standard deviations for each of these parameters.

## *Two-parameter fit*

In an alternative treatment, we assume that the dominant wave direction, $\theta^*$, as well as $K^*$, has been determined from the sideband frequencies, and use least-squares methods to estimate only the beamwidth and RMS waveheight. For a two-parameter fit there are two and six degrees of freedom for single and double beams, respectively, with corresponding values for $\chi^2_{0.95}$ of 6.0 and 12.6. The values of $I_{min}$ for the simulated data were 4.1 and 8.2; because these values are less than $\chi^2_{0.95}$, the model fit is considered satisfactory. The statistic Z is distributed as F(2,2) and $\frac{1}{3}$ F(2,6) for single and double beams; the 50% and 75% confidence contours are shown in fig. 9. It can be seen that the two-parameter fit gives results that are far more stable than

the three-parameter fit: h and $\Delta\theta^*$ are determined to 10 cm, 65° and 7 cm, 20° at the 75% confidence level (i.e., 2.4 standard deviations) for single and double beams, respectively.

We recommend using both the three-parameter and two-parameter fits to the sideband peak energy ratios--in conjunction with the determination of angle and period from the sideband centroid frequencies--and using the most accurate results. It turns out (for a single-beam radar) that when the dominant wave direction is almost perpendicular to the radar beam ($\theta^* \approx 90°$), the determination of angle from the centroid frequencies is extremely inaccurate, as can be seen from (89), whereas that obtained from the amplitude ratios is relatively well defined. When the dominant wave direction is along the radar beam, the opposite conclusion applies.

## 4.6 Interpretation Yielding Ocean-Wave Parameters as a Function of Wavenumber

With HF surface-wave radars, and occasionally with skywave radars when ionospheric contamination is very low, the resulting echo Doppler spectra are sufficiently crisp in frequency resolution to allow a determination of wave spectral information as a function of wave frequency (or wavenumber). In this case, we use least-squares methods to obtain the parameters of the cardioid model described in sec. 3.1 and written in normalized form in (76). In this sub-section it is therefore understood that the spreading factor s (and hence the half-power beamwidth $\Delta\theta^*$) and the dominant wave direction $\theta^*$ are functions of wavenumber. In the long-ocean wave region, we can also use the 'bands' approximation discussed in sec. 4.3: each frequency contour defines a narrow band of ocean wavenumbers, with the central wavenumber given in terms of the frequency displacement by

$$K \approx u^2 \quad . \tag{101}$$

Thus, to obtain ocean-wave model parameters at a particular value of K, one must fit the model to radar spectral values at the corresponding normalized Doppler frequency values from each Bragg line of u. For a single radar beam there are four such values corresponding to the four sidebands; for a double-beam system, eight. Substituting (76) into the linearized integral equation

(61) gives

$$R_{m,m'}(u) = F(u^2)\ \Psi_{m,m'}(u,\ \theta^*,\ \Delta\theta^*) \tag{102}$$

where

$$\Psi_{m,m'}(u,\ \theta^*,\ \Delta\theta^*) = \frac{2}{\int_{\pi}^{\pi} \cos^s(\frac{\theta}{2})d\theta} \int_0^{\infty} \int_{-\theta_L}^{\theta_L} |\gamma_L|^2\ \delta(mu + m' - m\sqrt{K} - m'\sqrt{K'}) \times \cos^s(\theta-\theta^*)\ \frac{K}{K'^4}\ dK d\theta\ , \tag{103}$$

and the spreading factor s is given in terms of $\Delta\theta^*$ by (92). $\theta_L$ is defined and discussed in sec. 3.6. Program 4 (Appendix E) calculates the elements $\Psi_{m,m'}(u,\ \theta^*,\ \Delta\theta^*)$ for a range of parameter values and an input value of u.

For each value of u in the range $0 < u < 0.25$, estimates of the parameters are obtained by minimizing the sum of squares of deviations given by

$$J(u) = \sum_{m,m'} \frac{(r_{m,m'}(u) - R_{m,m'}(u))^2}{\Delta r^2_{m,m'}(u)}\ . \tag{104}$$

The data values $r_{m,m'}(u)$ are the second-order spectral values of the data normalized by the first-order energy as defined in (61). The variance in the denominator is given very simply by

$$\Delta^2 r_{m,m'}(u) = \frac{r^2_{m,m'}(u)}{N_e} \tag{105}$$

where the effective number of spectral averages $N_e$ is given by

$$1/N_e = 1/N_1 + 1/N_2\ . \tag{106}$$

Here $N_1$ is the effective number of spectral samples in the first-order peak energy, defined in (96), and $N_2$ is the number of spectral averages in the second-order energy band at u of width $\Delta u$ given by (66). Methods described in Appendix A can be used to test the quality of the model fit and to place confidence limits on the derived parameters.

This procedure will give estimates of the normalized spectrum F(K), and also $\Delta\theta^*$ and $\theta^*$ as a function of normalized wavevector K in the range $0 < K < .06$. The ocean-wave nondirectional spatial spectrum is then

$$f(k) = (2k_o)^4 F(K) , \tag{107}$$

and the deep-water temporal spectrum at ocean-wave frequency $\nu$ (in Hz) is given by

$$T(\nu) = 4\pi \sqrt{gk^3}\, F(k) \tag{108}$$

where $\nu$ is given in terms of wavenumber k through the dispersion equation

$$\nu = \sqrt{gk}/2\pi . \tag{109}$$

For two beams, there is another set of equations for the power ratios:

$$R^{(2)}_{m,m'}(u) = F(K)\, \Psi_{m,m'}(u, \theta^* - \varepsilon, \Delta\theta^*) . \tag{110}$$

The sum of squared deviations now contains eight terms:

$$J(u) = \sum_{m,m';i=1,2} \frac{(r^{(i)}_{m,m'}(u) - R^{(i)}_{m,m'}(u))^2}{(\Delta r^2_{m,m'}(u))^{(i)}} \tag{111}$$

where the superscript i refers to the beam number.

Although we have not determined confidence intervals for simulated data, we can draw the following conclusions from the discussion of sec. 4.4 and the simulations described in sec. 4.5. For a single beam, the statistical uncertainties in ocean-wave parameters derived as a function of wavenumber will be large, unless the dominant wave direction is close to cross beam. Acceptable accuracies will result, however, if an estimate of ocean-wave direction can be made from the radar spectral peak frequencies or by some other means. Use of the peak frequency centroids for direction, of course, requires the assumption that this direction does not change significantly as a function of wave frequency in the long-wave region, and this may not be acceptable for some situations. For two radar beams it is not necessary to have an estimate of wave direction prior to using least-squares estimation. In this case, one

should be able to derive the nondirectional spectrum, the dominant ocean-wave direction, and beamwidth (the latter two vs. wave frequency) with good statistical accuracy.

# 5. CONCLUSIONS

In summary, we give in this report a detailed description of the computational and analytical techniques that have been developed for use with narrow-beam HF radar sea echo. We describe a method to calculate theoretical radar spectra for ocean waveheight directional spectral models, including the computer program that performs the calculation; these computations show that resulting theoretical radar spectra are sensitive to changes in the ocean-wave spectrum.

We then describe methods to give long-period ocean-wave parameters based on the interpretation of Barrick's equations for the first- and second-order radar cross section. The starting point in the data analysis is the combination of radar spectra from different ranges and times to produce minimum statistical variance in the composite spectrum. Least-squares methods are then used to estimate ocean-wave parameters by fitting cardioid models of the ocean-wave spectrum to the radar data. Computer programs are provided for the generation of grid-search elements. We discuss standard statistical methods for testing the quality of the model fit and for placing confidence limits on the derived parameters. These methods are easy to apply and should allow the routine derivation of long-period ocean-wave parameters--as well as their accuracy estimates--from narrow-beam radar sea echo.

A general conclusion is that the amount of accurate waveheight directional spectral information obtainable from a single, narrow-beam look at a patch of sea is limited. Not only is one constrained by the obvious left/right directional ambiguity about the look direction, but accurate measurement and separation of the waveheight nondirectional spectrum from wave beamwidth and wave mean direction becomes more difficult (except when mean wave direction is within 45° of the perpendicular to the radar beam). The example considered in this report shows an angular uncertainty of 70° and half-power beamwidth between 60° and 180° at the 50% confidence level for a 100-sample

spectral average. Furthermore, neglect of the latter two directional parameters in any inversion analysis does not mean one can then extract waveheight alone more accurately; such neglect will generally produce greater error or bias in waveheight.

Use of two radar beams to look at the sea from different directions not only eliminates the left/right ambiguity, but allows for accurate extraction of waveheight, mean wave direction, and wave beamwidth. If the sea-echo Doppler spectra are sufficiently crisp in frequency resolution (as with surface-wave radars), the latter two directional parameters can be derived as a function of wave frequency, as well as the nondirectional waveheight spectrum. However, two-beam radars have their own inherent disadvantages. For a single radar system that looks in two different directions, it must be assumed that the sea is statistically homogeneous within the two different patches; at best this can only be true with a short-range surface-wave radar where the patches are separated by no more than 30 km, and often it will not even then be true. On the other hand, two spatially separated (surface-wave or skywave) radars looking at the same patch of sea from different directions will certainly circumvent the homogeneity assumption, but at the cost and inconvenience of two radar systems.

## 6. ACKNOWLEDGMENTS

The authors are sincerely grateful to Dr. Lucy R. Wyatt of the University of Birmingham (U.K.) for a critical review of the analytical techniques and computer programs, which resulted in the correction of several errors and inconsistencies.

## 7. REFERENCES

Barrick, D. E., 1971. Theory of HF/VHF propagation across the rough sea: Parts 1 and 2. Radio Sci. 6:517-533.

Barrick, D. E., 1972a. First-order theory and analysis of MF/HF/VHF scatter from the sea. IEEE Trans. Antennas Propag. AP-20:2-10.

Barrick, D. E., 1972b. Remote sensing of sea state by radar. In Remote Sensing of the Troposphere, V. E. Derr (ed), NOAA/Environmental Research Laboratories, Boulder, Colo., (available U.S. Government Printing Office, Washington, D.C.), 12-1 to 12-46.

Barrick, D. E., 1977. The ocean waveheight nondirectional spectrum from inversion of the HF Doppler spectrum. Remote Sens. Environ. 6:201-227.

Barrick, D. E., 1980. Accuracy of parameter extraction from sample-averaged sea-echo Doppler spectra. IEEE Trans. Antennas Propag. AP-28:1-11.

Barrick, D. E., and B. J. Lipa, 1979. A compact transportable HF radar system for directional coastal wavefield measurements. In Ocean Wave Climate, M. D. Earle and A. Malahoff (eds.), Plenum, New York, 153-201.

Barrick, D. E., and J. B. Snider, 1977. The statistics of HF sea-echo Doppler spectra. IEEE Trans. Antennas Propag. AP-25:19-28.

Bevington, P. R., 1969. Data Reduction and Error Analysis for the Physical Sciences. McGraw-Hill, New York, 336 pp.

Brandt, S., 1970. Statistical and Computational Methods in Data Analysis. North-Holland, Amsterdam, 323 pp.

Jenkins, G. M., and D. G. Watts, 1968. Spectral Analysis and Its Applications. Holden-Day, San Francisco, Calif., 525 pp.

Lipa, B. J., and D. E. Barrick, 1980. Methods for the extraction of long period ocean wave parameters from narrow-beam HF radar sea echo. Radio Sci. 15:843-853.

Lipa, B. J., D. E. Barrick, and J. W. Maresca, Jr., 1981. HF radar measurements of long ocean waves. J. Geophys. Res. 86:4089-4102.

Phillips, O. M., 1977. The Dynamics of the Upper Ocean. Cambridge University Press, Cambridge, England, 336 pp.

# Appendix A: Nonlinear Least-Squares Estimation

Here we briefly describe nonlinear least-squares methods for the estimation of model parameters. In our problem, we wish to estimate n parameters $(x_j, j = 1,\ldots,n)$ from N data values $y_i$ through the equations

$$y_i = Y_i(x_1, x_2, \ldots, x_n), \quad i = 1,2,\ldots,N. \tag{A1}$$

Thus $Y_i(\cdot)$ defines a model for the value of the $i^{th}$ data point in terms of the parameters. The optimum solution is obtained by minimizing the weighted sum of squared deviations of the model values from the data

$$I = \sum_i \frac{(y_i - Y_i(x_1, \ldots, x_n))^2}{(\Delta y_i^2)} \tag{A2}$$

where the weight $(\Delta y_i^2)$ is the variance of $y_i$. The parameters defining the minimum value of I (which we term $I_{min}$) then have the minimum variance and are known as the least-squares estimates.

Bevington (1969) discusses statistical tests for the evaluation of least-squares estimation. Both I and $I_{min}$ are $\chi^2$ distributed; I has N degrees of freedom corresponding to the number of equations, $I_{min}$ has N-n degrees of freedom left after fitting n parameters to the N equations. If the fitting function (A1) is a good approximation to the data, the value of $I_{min}/(N-n)$ should be reasonably close to unity. If it is considerably larger, the deviations are too great, indicating that the fitting function is inappropriate. An objective limit to the value of $I_{min}$ is set by the $\chi^2$ test. A significance level, $\alpha$, (usually small) is chosen and the value of $I_{min}$ compared with the fractile $\chi^2_{(1-\alpha)}$ for (N-n) degrees of freedom. $\chi^2_{(1-\alpha)}$ is defined as follows: for a given number of degrees of freedom there is a probability $100(1-\alpha)\%$ that any random sample of data points will have a value of I at least as large as $\chi^2_{(1-\alpha)}$. Tables of $\chi^2_{(1-\alpha)}$ are available in most statistical texts. If $I_{min} \leq \chi^2_{(1-\alpha)}$, we conclude that the model fit is satisfactory. If $I_{min} \geq \chi^2_{(1-\alpha)}$, the deviations are too great and we must conclude that the model fit is unsatisfactory at this significance level.

Jenkins and Watts (1968) show that probability regions in parameter space are defined by contours of the parameter

$$Z = (I - I_{min})/I_{min} \quad . \tag{A3}$$

Because of the additive property of the $\chi^2$ distribution, the quantity $(I - I_{min})$ varies independently of $I_{min}$ and is $\chi^2$ distributed with n degrees of freedom. From the definition of the F-distribution, the $100(1-\alpha)\%$ confidence region in parameter space is defined by the contour

$$Z = \frac{n}{N-n} F(n,N-n;1-\alpha) \tag{A4}$$

where $F(n,N-n;1-\alpha)$ is the fractile of the F-distribution at significance level $\alpha$ and with degrees of freedom n and N-n.

# Appendix B: Program 1 and Sample Output

```
C
C       ------------------------------------------
C       ----------- PROGRAM 1 --------------------
C       ------------------------------------------
C
C       CALCULATES NORMALIZED COUPLING COEFFICIENT
C       INPUT: NORMALIZED WAVENO. K/(2*KO)
C
        IMPLICIT REAL(K)
        TYPE *,'-------------------------------------------------------'
        TYPE *,' -------------SAMPLE OUTPUT FROM PROGRAM 1-------------'
        TYPE *,'-------------------------------------------------------'
        TYPE *,' NORMALIZED WAVENO.'
        ACCEPT *,K
        Y=SQRT(K)
        DO 10 J=1,19
        TH=(J-1)*10*3.14159/180.
        G1=G(Y,TH,1)
        G2=G(Y,TH,2)
        THA=(J-1)*10
        WRITE(5,20)THA,G1,G2
20      FORMAT(' ANGLE',E11.3,' DEG.  COUP.COEFF: W**2>WB**2',E11.3
     C  ,'  W**2<WB**2',E11.3)
10      CONTINUE
        END
C
C       G IS THE COUPLING COEFFICIENT
C
        FUNCTION G(Y,TH,MM)
        IMPLICIT REAL (K)
        COMPLEX CH,CE
        M=-2*MM+3
        CT=COS(TH)
        Y2=Y*Y
        Y4=Y2*Y2
        YP2=SQRT(1.+2.*Y2*CT+Y4)
        YP=SQRT(YP2)
        X=((M*Y+YP)**2+1.)/((M*Y+YP)**2-1.)
C       CH, CE ARE THE HYDRODYNAMIC,ELECTROMAGNETIC COMPONENTS
        CH=(0.,-1.)*(Y2+YP2-(Y*YP2+Y*CT+Y*Y2)*X/(M*YP))
        CE=(Y2*CT+Y4*(2.-CT**2))/(CSQRT(CMPLX(-Y2*CT-Y4,0.))+(.011,-.012)/2.)
        CH=CH/2.
        CE=CE/2.
        G=CABS(CH+CE)**2
        RETURN
        END


        End Program 1
```

```
 ------------------------------------------------------
 ------------SAMPLE OUTPUT FROM PROGRAM 1-----------
------------------------------------------------------
 NORMALIZED WAVENO.
.05
ANGLE  0.000E+00 DEG.  COUP.COEFF: W**2>WB**2  0.146E+00  W**2<WB**2  0.146E+00
ANGLE  0.100E+02 DEG.  COUP.COEFF: W**2>WB**2  0.142E+00  W**2<WB**2  0.140E+00
ANGLE  0.200E+02 DEG.  COUP.COEFF: W**2>WB**2  0.131E+00  W**2<WB**2  0.122E+00
ANGLE  0.300E+02 DEG.  COUP.COEFF: W**2>WB**2  0.112E+00  W**2<WB**2  0.949E-01
ANGLE  0.400E+02 DEG.  COUP.COEFF: W**2>WB**2  0.898E-01  W**2<WB**2  0.647E-01
ANGLE  0.500E+02 DEG.  COUP.COEFF: W**2>WB**2  0.650E-01  W**2<WB**2  0.362E-01
ANGLE  0.600E+02 DEG.  COUP.COEFF: W**2>WB**2  0.408E-01  W**2<WB**2  0.142E-01
ANGLE  0.700E+02 DEG.  COUP.COEFF: W**2>WB**2  0.203E-01  W**2<WB**2  0.196E-02
ANGLE  0.800E+02 DEG.  COUP.COEFF: W**2>WB**2  0.613E-02  W**2<WB**2  0.948E-03
ANGLE  0.900E+02 DEG.  COUP.COEFF: W**2>WB**2  0.967E-04  W**2<WB**2  0.113E-01
ANGLE  0.100E+03 DEG.  COUP.COEFF: W**2>WB**2  0.116E-02  W**2<WB**2  0.191E-01
ANGLE  0.110E+03 DEG.  COUP.COEFF: W**2>WB**2  0.156E-01  W**2<WB**2  0.493E-01
ANGLE  0.120E+03 DEG.  COUP.COEFF: W**2>WB**2  0.450E-01  W**2<WB**2  0.878E-01
ANGLE  0.130E+03 DEG.  COUP.COEFF: W**2>WB**2  0.865E-01  W**2<WB**2  0.130E+00
ANGLE  0.140E+03 DEG.  COUP.COEFF: W**2>WB**2  0.135E+00  W**2<WB**2  0.172E+00
ANGLE  0.150E+03 DEG.  COUP.COEFF: W**2>WB**2  0.184E+00  W**2<WB**2  0.210E+00
ANGLE  0.160E+03 DEG.  COUP.COEFF: W**2>WB**2  0.226E+00  W**2<WB**2  0.239E+00
ANGLE  0.170E+03 DEG.  COUP.COEFF: W**2>WB**2  0.254E+00  W**2<WB**2  0.258E+00
ANGLE  0.180E+03 DEG.  COUP.COEFF: W**2>WB**2  0.264E+00  W**2<WB**2  0.264E+00
```

# Appendix C: Program 2 and Sample Output

```
C       ------------------------------------------
C       -------------- PROGRAM 2 -----------------
C       ------------------------------------------
C       CALCULATION OF PRODUCT OF SECOND ORDER RADAR CROSS SECTION
C       AND THE BRAGG FREQ
C       FOR A PHILLIPS SPECTRUM, CARDIOID DIRECTIONAL DIST.
C
C       INPUT : KC= CUTOFF WAVENO./(2*RADAR WAVENO.)
C               TO=DOMINANT DIRECTION (DEG. REL. TO RADAR BEAM)
C               S=SPREADING FACTOR
C               NQ=NO. QUADRATURE POINTS
C
C       OUTPUT : NORMALIZED 2CND ORDER SPECTRUM DEFINED IN EQ.39
C       FOR NORMALIZED FREQUENCIES BETWEEN -2 AND +2
C
        IMPLICIT REAL(K)
        COMMON S,KC,AS
        PI=3.14159
        TYPE *,' ------------------------------------------------------'
        TYPE *,' -------- SAMPLE OUTPUT FROM PROGRAM 2 ---------------'
        TYPE *,' ------------------------------------------------------'
        TYPE *,' KC,TO,S,NQ'
        ACCEPT *,KC,TO,S,NQ
        NQQ=NQ
        TO=TO*3.14159/180.
C
C       CALCULATION OF INTEGRAL COS(THETA/2)**S OVER THETA
C
        AS=0
        DO 20 J=1,NQ
        TH=(J-1)*2*PI/NQ
        SP=ABS(COS(TH/2))
        IF(SP.EQ.0.)GO TO 111
        IF(ALOG10(SP)*S.GT.-10.)H=SP**S
        IF(ALOG10(SP)*S.LE.-10.)H=0
        SP=H
        AS=AS+SP
111     CONTINUE
20      CONTINUE
        AS=AS*2*PI/NQ
        WRITE(5,123)AS
123     FORMAT(' INTEGRAL',E11.3)
C       START OF DOPPLER LOOP
        DO 2000 NF=1,60
        E=-2+(NF-1)*4/60.                !NORMALIZED DOPPLER
        IF(ABS(E).EQ.1.)GO TO 11
        IF(ABS(E).LT..25)GO TO 11
        NQ=NQQ
        IF(ABS(ABS(E)-2.**.75).LT.0.15)NQ=4*NQQ
        IF(E.GT.0.)NFREQ=1
        IF(E.LE.0.)NFREQ=2
        U=ABS(E)-1
        IF(U.LT.0.)M=2  !PARAMETER L DEFINED IN EQ.(32) IS (-2*M+3)
        IF(U.GE.0.)M=1
        U=ABS(U)
        UP=PI           !SETS UPPER LIMIT ON THETA INTEGRATION
        IF(ABS(E).GE.SQRT(2.))UP=PI-ACOS(2/E**2)
        F=0
        IF(M.EQ.1)EST=(U**2+2*U)/(2*(U+1))  !EXACT SOLUTION FOR Y AT THETA=0
        IF(M.EQ.2)EST=(U-1+SQRT(1+2*U-U**2))/2.  !EXACT AT THETA=PI
```

```
      DO 30 II=1,NQ                                    !START THETA LOOP
      IF(M.EQ.1)TH=(II-1)*UP/(NQ-1.)
      IF(M.EQ.2)TH=PI-(II-1)*PI/(NQ-1.)
      Y=TY(M,U,TH,EST)
      EST=Y
      IF(Y.GT.4.)F2=0.
      IF(Y.GT.4.)GO TO 21
      F=F+G(Y,TH,M,NFREQ,T0)
      IF(II.EQ.1)F1=FACT
      IF(II.EQ.NQ)F2=FACT
30    CONTINUE
21    CONTINUE
      F=(F-F1/2.-F2/2.)*UP/(NQ-1.)
      F=F*2**3*PI
      WRITE(5,70)NF,E,F
70    FORMAT(1X,I4,7E11.3)
11    CONTINUE
2000  CONTINUE                                         !END DOPPLER LOOP
      END
C
C     SPEC IS THE OCEAN WAVE SPECTRUM
C
      FUNCTION SPEC(TH,T0,K)
      IMPLICIT REAL(K)
      COMMON S,KC,AS
      IF(K.LE.KC)SPEC=0
      IF(K.LE.KC)GO TO 20
      G=ABS(COS((TH-T0)/2))
      IF(G.EQ.0.)GO TO 10
      IF(ALOG10(G)*S.GT.-10.)H=G**S
      IF(ALOG10(G)*S.LE.-10.)H=0
      G=H
10    CONTINUE
      SPEC=.005*G/(AS*K**4)
20    CONTINUE
      RETURN
      END
```

{FACT = G(Y,TH,M,NFREQ,TØ)
{F = F + FACT

```
C
C       G IS THE PRODUCT OF THE COUPLING COEFFICIENT , THE JACOBIANS
C       AND THE OCEAN SPECTRAL FACTORS
C
        FUNCTION G(Y,TH,MM,NFREQ,T0)
        IMPLICIT REAL (K)
        COMPLEX CH,CE
        COMMON S,KC,AS
        PI=3.14159
        M=-2*MM+3
        CT=COS(TH)
        Y2=Y*Y
        Y4=Y2*Y2
        YP2=SQRT(1.+2.*Y2*CT+Y4)
        YP=SQRT(YP2)
        FACT=(1+Y2*CT)/YP2
        IF(ABS(FACT).LE.1.)THD=ACOS(FACT)
        IF(FACT.GT.1.)THD=0
        IF(FACT.LT.-1.)THD=PI
        THD=THD+PI
        X=((Y+M*YP)**2+1.)/((Y+M*YP)**2-1.)
        CH=(0.,-1.)*(Y2+YP2-(Y*YP2+Y*CT+Y*Y2)*X/(M*YP))
        CE=(Y2*CT+Y4*(2.-CT**2))/(CSQRT(CMPLX(-Y2*CT-Y4,0.))+(.011,-.012)/2.)
        CH=CH/2.
        CE=CE/2.
        G1=CABS(CH+CE)**2                          !COUPLING COEFF
        XJ=Y**3*2/ABS(1.+M*(Y2*Y+Y*CT)/(YP2*YP))                !JACOBIANS
        IF(NFREQ.EQ.1)SP2=SPEC(THD,T0,YP2)         !SPECTRAL FACTORS
        IF(NFREQ.EQ.2)SP2=SPEC(THD,T0+PI,YP2)
        IF(NFREQ.EQ.MM)SP1=SPEC(TH,T0,Y2)
        IF(NFREQ.NE.MM)SP1=SPEC(TH,T0+PI,Y2)
        IF(NFREQ.EQ.1)SP3=SPEC(-THD,T0,YP2)
        IF(NFREQ.EQ.2)SP3=SPEC(-THD,T0+PI,YP2)
        IF(NFREQ.EQ.MM)SP4=SPEC(-TH,T0,Y2)
        IF(NFREQ.NE.MM)SP4=SPEC(-TH,T0+PI,Y2)
        G=G1*XJ*(SP1*SP2+SP3*SP4)
        RETURN
        END
C       TY IS THE SOLUTION OF THE DELTA FN. CONSTRAINT TO GIVE Y=SQRT(K/2)
C       FOR A GIVEN ANGLE, DOPPLER. EST IS AN ESTIMATE OF Y.
        FUNCTION TY(M,U,TH,EST)
        M1=-2*M+3
        CT=COS(TH)
        Y0=EST
1       FY0=Y0+M1*(1.+2.*Y0*Y0*CT+Y0**4)**.25-U-M1
        FY0P=1.+M1*(Y0**3+Y0*CT)/(1.+2.*Y0*Y0*CT+Y0**4)**.75
        Y1=Y0-FY0/FY0P
        T=ABS((Y1-Y0)/Y0)
        Y0=Y1
        IF (T.GT.0.0001)GOTO 1
        TY=Y1
        RETURN
        END
```

End Program 2

```
 ------------------------------------------------
 -------- SAMPLE OUTPUT FROM PROGRAM 2 ----------
 ------------------------------------------------
 KC,T0,S,NQ
,03,45.,4.,19
INTEGRAL  0.236E+01
   1 -0.200E+01  0.888E-05
   2 -0.193E+01  0.135E-04
   3 -0.187E+01  0.221E-04
   4 -0.180E+01  0.358E-04
   5 -0.173E+01  0.830E-04
   6 -0.167E+01  0.593E-03
   7 -0.160E+01  0.349E-03
   8 -0.153E+01  0.245E-03
   9 -0.147E+01  0.162E-02
  10 -0.140E+01  0.101E-01
  11 -0.133E+01  0.135E-01
  12 -0.127E+01  0.355E-01
  13 -0.120E+01  0.144E+00
  14 -0.113E+01  0.000E+00
  15 -0.107E+01  0.000E+00
  17 -0.933E+00  0.000E+00
  18 -0.867E+00  0.000E+00
  19 -0.800E+00  0.752E-01
  20 -0.733E+00  0.140E-01
  21 -0.667E+00  0.412E-02
  22 -0.600E+00  0.187E-02
  23 -0.533E+00  0.130E-02
  24 -0.467E+00  0.868E-03
  25 -0.400E+00  0.728E-03
  26 -0.333E+00  0.611E-03
  27 -0.267E+00  0.460E-03
  35  0.267E+00  0.164E-03
  36  0.333E+00  0.178E-03
  37  0.400E+00  0.192E-03
  38  0.467E+00  0.224E-03
  39  0.533E+00  0.317E-03
  40  0.600E+00  0.483E-03
  41  0.667E+00  0.914E-03
  42  0.733E+00  0.220E-02
  43  0.800E+00  0.752E-02
  44  0.867E+00  0.000E+00
  45  0.933E+00  0.000E+00
  47  0.107E+01  0.000E+00
  48  0.113E+01  0.000E+00
  49  0.120E+01  0.360E-02
  50  0.127E+01  0.717E-03
  51  0.133E+01  0.191E-03
  52  0.140E+01  0.651E-04
  53  0.147E+01  0.192E-04
  54  0.153E+01  0.659E-05
  55  0.160E+01  0.266E-05
  56  0.167E+01  0.967E-06
  57  0.173E+01  0.389E-06
  58  0.180E+01  0.186E-06
  59  0.187E+01  0.123E-06
  60  0.193E+01  0.102E-06
```

# Appendix D: Program 3 and Sample Output

```
C       ------------------------------------
C       --------- PROGRAM 3 ----------------
C       ------------------------------------
C       CALCULATION OF GRID SEARCH ELEMENTS FOR SINGLE DOMINANT
C       OCEAN WAVELENGTH
C
C       INPUT : K = OCEAN WAVENO. /(2*RADAR WAVENO.) (MUST BE < .06)
C
C       OUTPUT : GRID SEARCH ELEMENTS DEFINED IN EQ. 91 FOR THE FOUR SIDEBANDS,
C                FOR A RANGE OF OCEAN WAVE DIRECTIONS AND BEAMWIDTHS
C                (STORED IN ARRAY H)
C
        IMPLICIT REAL(K)
        DIMENSION F(4),H(7,7,4)
        PI=3.14159
        TYPE *,' ------------------------------------------------'
        TYPE *,' ---------- SAMPLE OUTPUT FROM PROGRAM 3 ----------'
        TYPE *,' ------------------------------------------------'
        TYPE *,' K'
        ACCEPT *,K
        Y=SQRT(K)                               !DEFINITION OF PARAMETER Y
        DO 1000 NTO=1,7                         ! DEFINES OCEAN WAVE DIR.
        TO=PI+(NTO-1)*PI/12
        DO 2000 NS=1,6                          ! DEFINES OCEAN WAVE BEAMWIDTH
        B=180-(NS-1)*30                         ! HALF POWER BEAMWIDTH
        NQ=30*360/B                             ! NO. QUADRATURE PTS.
        BB=B
        B=B*PI/180.
        S=ALOG10(.5)/ALOG10(COS(B/4.))          ! SPREADING FACTOR
C
C       CALCULATION OF INTEGRAL COS(THETA/2)**S OVER THETA
C
        AS=0
        DO 20 J=1,NQ
        TH=(J-1)*2*PI/NQ
        AS=AS+SPEC(TH,S)
20      CONTINUE
        AS=AS*2*PI/NQ
C
C       CALCULATION OF FACTOR IN EQ. 91 FOR 4 SIDEBANDS, CARDIOID MODEL
C       DEFINED BY IND=M+(NFREQ-1)*2
C       M=(1,2) FOR (OUTER,INNER) SIDE OF BRAGG LINE
C       NFREQ=(1,2) FOR (POSITIVE,NEG.) DOPPLER
C
        DO 50 J=1,4                                 ! INITIALIZATION
        F(J)=0
50      CONTINUE
        DO 30 II=1,NQ                               !START THETA LOOP
        TH=(II-1)*2*PI/NQ
        G1=SPEC(TH-TO,S)
        G2=SPEC(TH-TO-PI,S)
        DO 40 M=1,2
        DO 40 NFREQ=1,2
        IND=NFREQ+(M-1)*2
C       OCEAN SPECTRAL FACTORS
        IF(NFREQ.EQ.M)SF=G1/AS
        IF(NFREQ.NE.M)SF=G2/AS
        F(IND)=F(IND)+G(Y,TH,M)*SF*2
40      CONTINUE
30      CONTINUE
```

```
      DO 60 J=1,4
      F(J)=F(J)*2*PI/NQ
      H(NTO,NS,J)=F(J)                        ! H ARE GRID SEARCH ELEMENTS
60    CONTINUE
      ATO=TO*180/PI
      WRITE(5,70)S,ATO,(F(J),J=1,4)
      WRITE(1,70)K,BB,ATO,(F(J),J=1,4)
70    FORMAT(1X,7E11.3)
2000  CONTINUE                                  !END BEAMWIDTH LOOP
C
C     CALCULATION OF FACTOR IN EQ. 91 FOR AN IMPULSE FUNCTION IN DIRECTION
C
      DO 21 M=1,2
      DO 21 NFREQ=1,2
      S=1.E+4
      BB=0
      IND=NFREQ+(M-1)*2
      IF(NFREQ.EQ.M)F(IND)=G(Y,TO,M)*2
      IF(NFREQ.NE.M)F(IND)=G(Y,TO+PI,M)*2
      H(NTO,7,IND)=F(IND)
21    CONTINUE
      WRITE(5,70)S,ATO,(F(J),J=1,4)
1000  CONTINUE                                  !END DIRECTION LOOP
      END
C
C     SPEC IS THE DIRECTIONAL DISTRIBUTION  COS(TH/2)**S
C
      FUNCTION SPEC(TH,S)
      G=ABS(COS(TH/2))
      IF(G.EQ.0.)GO TO 10
      IF(ALOG10(G)*S.GT.-10.)H=G**S
      IF(ALOG10(G)*S.LE.-10.)H=0
      G=H
10    CONTINUE
      SPEC=G
      RETURN
      END
C
C     G IS THE PRODUCT OF THE COUPLING COEFFICIENT AND THE RESIDUAL
C     WAVENUMBER FACTOR
C
      FUNCTION G(Y,TH,MM)
      IMPLICIT REAL (K)
      COMPLEX CH,CE
      M=-2*MM+3
      CT=COS(TH)
      Y2=Y*Y
      Y4=Y2*Y2
      YP2=SQRT(1.+2.*Y2*CT+Y4)
      YP=SQRT(YP2)
      YP4=YP2*YP2
      RR=1/YP4**2                             ! RESIDUAL WAVENUMBER FACTOR
      X=((Y+M*YP)**2+1.)/((Y+M*YP)**2-1.)
      CH=(0.,-1.)*(Y2+YP2-(Y*YP2+Y*CT+Y*Y2)*X/(M*YP))
      CE=(Y2*CT*2+Y4*(2.-CT**2))/(CSQRT(CMPLX(-Y2*CT-Y4,0.))+(.011,-.012)/2.)
      CH=CH/2.
      CE=CE/2.
      G=CABS(CH+CE)**2                          !COUPLING COEFF
      G=G*RR
      RETURN
      END
      End Program 3
```

---

---------- SAMPLE OUTPUT FROM PROGRAM 3 ----------

---

K

.05

| | | | | | |
|---|---|---|---|---|---|
| 0.200E+01 | 0.180E+03 | 0.324E+00 | 0.782E-01 | 0.788E-01 | 0.368E+00 |
| 0.299E+01 | 0.180E+03 | 0.367E+00 | 0.730E-01 | 0.678E-01 | 0.414E+00 |
| 0.482E+01 | 0.180E+03 | 0.426E+00 | 0.755E-01 | 0.651E-01 | 0.475E+00 |
| 0.875E+01 | 0.180E+03 | 0.505E+00 | 0.860E-01 | 0.729E-01 | 0.552E+00 |
| 0.200E+02 | 0.180E+03 | 0.605E+00 | 0.101E+00 | 0.903E-01 | 0.639E+00 |
| 0.807E+02 | 0.180E+03 | 0.702E+00 | 0.115E+00 | 0.111E+00 | 0.714E+00 |
| 0.100E+05 | 0.180E+03 | 0.745E+00 | 0.120E+00 | 0.120E+00 | 0.745E+00 |
| 0.200E+01 | 0.195E+03 | 0.320E+00 | 0.824E-01 | 0.837E-01 | 0.363E+00 |
| 0.299E+01 | 0.195E+03 | 0.360E+00 | 0.753E-01 | 0.713E-01 | 0.406E+00 |
| 0.482E+01 | 0.195E+03 | 0.413E+00 | 0.751E-01 | 0.659E-01 | 0.462E+00 |
| 0.875E+01 | 0.195E+03 | 0.483E+00 | 0.828E-01 | 0.702E-01 | 0.531E+00 |
| 0.200E+02 | 0.195E+03 | 0.568E+00 | 0.955E-01 | 0.832E-01 | 0.608E+00 |
| 0.807E+02 | 0.195E+03 | 0.647E+00 | 0.108E+00 | 0.988E-01 | 0.674E+00 |
| 0.100E+05 | 0.195E+03 | 0.682E+00 | 0.112E+00 | 0.106E+00 | 0.701E+00 |
| 0.200E+01 | 0.210E+03 | 0.308E+00 | 0.947E-01 | 0.982E-01 | 0.349E+00 |
| 0.299E+01 | 0.210E+03 | 0.338E+00 | 0.828E-01 | 0.820E-01 | 0.383E+00 |
| 0.482E+01 | 0.210E+03 | 0.377E+00 | 0.753E-01 | 0.697E-01 | 0.424E+00 |
| 0.875E+01 | 0.210E+03 | 0.422E+00 | 0.746E-01 | 0.638E-01 | 0.472E+00 |
| 0.200E+02 | 0.210E+03 | 0.468E+00 | 0.803E-01 | 0.651E-01 | 0.522E+00 |
| 0.807E+02 | 0.210E+03 | 0.505E+00 | 0.872E-01 | 0.685E-01 | 0.564E+00 |
| 0.100E+05 | 0.210E+03 | 0.518E+00 | 0.903E-01 | 0.702E-01 | 0.580E+00 |
| 0.200E+01 | 0.225E+03 | 0.288E+00 | 0.114E+00 | 0.121E+00 | 0.326E+00 |
| 0.299E+01 | 0.225E+03 | 0.306E+00 | 0.965E-01 | 0.101E+00 | 0.346E+00 |
| 0.482E+01 | 0.225E+03 | 0.324E+00 | 0.791E-01 | 0.792E-01 | 0.368E+00 |
| 0.875E+01 | 0.225E+03 | 0.336E+00 | 0.659E-01 | 0.595E-01 | 0.387E+00 |
| 0.200E+02 | 0.225E+03 | 0.337E+00 | 0.599E-01 | 0.448E-01 | 0.401E+00 |
| 0.807E+02 | 0.225E+03 | 0.324E+00 | 0.592E-01 | 0.343E-01 | 0.409E+00 |
| 0.100E+05 | 0.225E+03 | 0.316E+00 | 0.593E-01 | 0.293E-01 | 0.412E+00 |
| 0.200E+01 | 0.240E+03 | 0.263E+00 | 0.140E+00 | 0.151E+00 | 0.296E+00 |
| 0.299E+01 | 0.240E+03 | 0.266E+00 | 0.118E+00 | 0.128E+00 | 0.302E+00 |
| 0.482E+01 | 0.240E+03 | 0.262E+00 | 0.908E-01 | 0.984E-01 | 0.302E+00 |
| 0.875E+01 | 0.240E+03 | 0.245E+00 | 0.633E-01 | 0.650E-01 | 0.293E+00 |
| 0.200E+02 | 0.240E+03 | 0.209E+00 | 0.419E-01 | 0.336E-01 | 0.272E+00 |
| 0.807E+02 | 0.240E+03 | 0.163E+00 | 0.312E-01 | 0.122E-01 | 0.246E+00 |
| 0.100E+05 | 0.240E+03 | 0.140E+00 | 0.278E-01 | 0.308E-02 | 0.235E+00 |
| 0.200E+01 | 0.255E+03 | 0.233E+00 | 0.169E+00 | 0.186E+00 | 0.261E+00 |
| 0.299E+01 | 0.255E+03 | 0.224E+00 | 0.147E+00 | 0.163E+00 | 0.253E+00 |
| 0.482E+01 | 0.255E+03 | 0.203E+00 | 0.114E+00 | 0.130E+00 | 0.236E+00 |
| 0.875E+01 | 0.255E+03 | 0.165E+00 | 0.748E-01 | 0.881E-01 | 0.204E+00 |
| 0.200E+02 | 0.255E+03 | 0.112E+00 | 0.362E-01 | 0.429E-01 | 0.161E+00 |
| 0.807E+02 | 0.255E+03 | 0.573E-01 | 0.123E-01 | 0.114E-01 | 0.113E+00 |
| 0.100E+05 | 0.255E+03 | 0.313E-01 | 0.605E-02 | 0.443E-02 | 0.884E-01 |
| 0.200E+01 | 0.270E+03 | 0.201E+00 | 0.201E+00 | 0.223E+00 | 0.223E+00 |
| 0.299E+01 | 0.270E+03 | 0.183E+00 | 0.183E+00 | 0.206E+00 | 0.206E+00 |
| 0.482E+01 | 0.270E+03 | 0.152E+00 | 0.152E+00 | 0.177E+00 | 0.177E+00 |
| 0.875E+01 | 0.270E+03 | 0.108E+00 | 0.108E+00 | 0.134E+00 | 0.134E+00 |
| 0.200E+02 | 0.270E+03 | 0.556E-01 | 0.556E-01 | 0.831E-01 | 0.831E-01 |
| 0.807E+02 | 0.270E+03 | 0.139E-01 | 0.139E-01 | 0.376E-01 | 0.376E-01 |
| 0.100E+05 | 0.270E+03 | 0.193E-03 | 0.192E-03 | 0.225E-01 | 0.225E-01 |

# Appendix E: Program 4 and Sample Output

```
C
C       ------------------------------
C       --------- PROGRAM 4 ---------
C       ------------------------------
C
C       CALCULATION OF GRID SEARCH ELEMENTS FOR RANGE OF OCEAN WAVELENGTHS
C
C       INPUT : U=NORMALIZED SHIFT FROM BRAGG FREQENCY
C                =ABS(ABS(W)/WB-1)   , (MUST BE < 0.25)
C
C       OUTPUT : GRID SEARCH ELEMENTS (EQ.103) FOR THE FOUR SIDEBANDS,
C                AND A RANGE OF OCEAN WAVE DIRECTIONS AND BEAMWIDTHS
C               (STORED IN ARRAY H)
C
        IMPLICIT REAL(K)
        DIMENSION F(4),H(7,7,4)
        PI=3.14159
        TYPE *,'-------------------------------------------------'
        TYPE *,'---------- SAMPLE OUTPUT FROM PROGRAM 4 ----------'
        TYPE *,'-------------------------------------------------'
        TYPE *,' U'
        ACCEPT *,U
C
C       CALCULATES OCEAN WAVENO. BAND
        KU=(U**2+U**3)
        KL=(U**2-U**3)
        WRITE(5,682)KL,KU
682     FORMAT(' NORMALIZED WAVENO. BAND',2E11.3)
        DO 1000 NT0=1,7                         ! DEFINES OCEAN WAVE DIR.
        T0=PI+(NT0-1)*PI/12
        DO 2000 NS=1,6                          ! DEFINES OCEAN WAVE BEAMWIDTH
        B=180-(NS-1)*30                         ! HALF POWER BEAMWIDTH
        NQ=30*360/B                             ! NO. QUADRATURE PTS.
        B=B*PI/180.
        S=ALOG10(.5)/ALOG10(COS(B/4.))          ! SPREADING FACTOR
C
C       CALCULATION OF INTEGRAL COS(THETA/2)**S OVER THETA
C
        AS=0
        DO 20 J=1,NQ
        TH=(J-1)*2*PI/NQ
        AS=AS+SPEC(TH,S)
20      CONTINUE
        AS=AS*2*PI/NQ
C
C       CALCULATION OF FACTOR DEFINED IN EQ(103) , CARDIOID MODEL
C       FOR 4 SIADEBANDS DEFINED BY IND=M+(NFREQ-1)*2
C       M=(1,2) FOR (OUTER,INNER) SIDE OF BRAGG LINE
C       NFREQ=(1,2) FOR (POSITIVE,NEG.) DOPPLER
C
        DO 50 J=1,4                                 ! INITIALIZATION
        F(J)=0
50      CONTINUE
```

```
      DO 30 II=1,NQ                                  !START THETA LOOP
      TH=(II-1)*2*PI/NQ
      G1=SPEC(TH-T0,S)
      G2=SPEC(TH-T0-PI,S)
      DO 40 M=1,2
      Y=TY(M,U,TH)
      DO 40 NFREQ=1,2
      IND=NFREQ+(M-1)*2
C     OCEAN SPECTRAL FACTORS
      IF(NFREQ.EQ.M)SP=G1/AS
      IF(NFREQ.NE.M)SP=G2/AS
      F(IND)=F(IND)+G(Y,TH,M)*SP*2
40    CONTINUE
30    CONTINUE
      DO 60 J=1,4
      F(J)=F(J)*2*PI/NQ
      H(NT0,NS,J)=F(J)                          ! H ARE GRID SEARCH ELEMENTS
60    CONTINUE
      AT0=T0*180/PI
      WRITE(5,70)S,AT0,(F(J),J=1,4)
70    FORMAT(1X,7E11.3)
2000  CONTINUE                                       !END BEAMWIDTH LOOP
C
C     CALCULATION OF FACTOR DEFINED IN EQ.(103)
C     FOR AN IMPULSE FUNCTION IN DIRECTION
C
      DO 21 M=1,2
      DO 21 NFREQ=1,2
      S=1.E+4
      BB=0
      IND=NFREQ+(M-1)*2
      IF(NFREQ.EQ.M)F(IND)=G(Y,T0,M)*2
      IF(NFREQ.NE.M)F(IND)=G(Y,T0+PI,M)*2
      H(NT0,7,IND)=F(IND)
21    CONTINUE
      WRITE(5,70)S,AT0,(F(J),J=1,4)
1000  CONTINUE                                       !END DIRECTION LOOP
      END
C
C     SPEC IS THE DIRECTIONAL DISTRIBUTION  COS(TH/2)**S
C
      FUNCTION SPEC(TH,S)
      G=ABS(COS(TH/2))
      IF(G.EQ.0.)GO TO 10
      IF(ALOG10(G)*S.GT.-10.)H=G**S
      IF(ALOG10(G)*S.LE.-10.)H=0
      G=H
10    CONTINUE
      SPEC=G
      RETURN
      END
```

```
C
C       G IS THE PRODUCT OF THE COUPLING COEFFICIENT , THE RESIDUAL
C       WAVENUMBER FACTOR AND THE JACOBIANS
C
        FUNCTION G(Y,TH,MM)
        IMPLICIT REAL (K)
        COMPLEX CH,CE
        M=-2*MM+3
        CT=COS(TH)
        Y2=Y*Y
        Y4=Y2*Y2
        YP2=SQRT(1.+2.*Y2*CT+Y4)
        YP=SQRT(YP2)
        YP4=YP2*YP2
        RR=1/YP4**2                              ! RESIDUAL WAVENUMBER FACTOR
        X=((Y+M*YP)**2+1.)/((Y+M*YP)**2-1.)
        CH=(0.,-1.)*(Y2+YP2-(Y*YP2+Y*CT+Y*Y2)*X/(M*YP))
        CE=(Y2*CT+Y4*(2.-CT**2))/(CSQRT(CMPLX(-Y2*CT-Y4,0.))+(.011,-.012)/2.)
        CH=CH/2
        CE=CE/2.
        G=CABS(CH+CE)**2                          !COUPLING COEFF
        XJ=Y**3*2/ABS(1.+M*(Y2*Y+Y*CT)/(YP2*YP))          !JACOBIANS
        G=G*RR*XJ
        RETURN
        END
C
C       TY SOLVES EQUATION 43 BY A NEWTON-RAPHSON METHOD
C       TO GIVE Y=SQRT(K/2.) FOR A GIVEN ANGLE, DOPPLER
        FUNCTION TY(M,U,TH)
        M1=-2*M+3
        CT=COS(TH)
        YO=U
1       FYO=YO+M1*(1.+2.*YO*YO*CT+YO**4)**.25-U-M1
        FYOP=1.+M1*(YO**3+YO*CT)/(1.+2.*YO*YO*CT+YO**4)**.75
        Y1=YO-FYO/FYOP
        T=ABS((Y1-YO)/YO)
        YO=Y1
        IF (T.GT.0.0001)GOTO 1
        TY=Y1
        RETURN
        END

        End Program 4
```

```
 ------------------------------------------------
--------- SAMPLE OUTPUT FROM PROGRAM 4 ---------
------------------------------------------------
 U
.1
NORMALIZED WAVENO. BAND  0.900E-02  0.110E-01
  0.200E+01   0.180E+03  0.627E-03  0.342E-03  0.456E-03  0.442E-03
  0.299E+01   0.180E+03  0.698E-03  0.358E-03  0.495E-03  0.480E-03
  0.482E+01   0.180E+03  0.803E-03  0.396E-03  0.563E-03  0.541E-03
  0.875E+01   0.180E+03  0.951E-03  0.457E-03  0.665E-03  0.626E-03
  0.200E+02   0.180E+03  0.114E-02  0.531E-03  0.800E-03  0.724E-03
  0.807E+02   0.180E+03  0.132E-02  0.593E-03  0.932E-03  0.806E-03
  0.100E+05   0.180E+03  0.140E-02  0.803E-03  0.991E-03  0.113E-02
  0.200E+01   0.195E+03  0.622E-03  0.347E-03  0.455E-03  0.442E-03
  0.299E+01   0.195E+03  0.686E-03  0.358E-03  0.490E-03  0.475E-03
  0.482E+01   0.195E+03  0.780E-03  0.388E-03  0.548E-03  0.528E-03
  0.875E+01   0.195E+03  0.909E-03  0.440E-03  0.636E-03  0.602E-03
  0.200E+02   0.195E+03  0.107E-02  0.505E-03  0.749E-03  0.689E-03
  0.807E+02   0.195E+03  0.122E-02  0.560E-03  0.858E-03  0.763E-03
  0.100E+05   0.195E+03  0.129E-02  0.755E-03  0.910E-03  0.107E-02
  0.200E+01   0.210E+03  0.608E-03  0.362E-03  0.455E-03  0.443E-03
  0.299E+01   0.210E+03  0.654E-03  0.359E-03  0.475E-03  0.461E-03
  0.482E+01   0.210E+03  0.716E-03  0.368E-03  0.509E-03  0.492E-03
  0.875E+01   0.210E+03  0.795E-03  0.393E-03  0.557E-03  0.537E-03
  0.200E+02   0.210E+03  0.880E-03  0.432E-03  0.614E-03  0.592E-03
  0.807E+02   0.210E+03  0.949E-03  0.469E-03  0.663E-03  0.642E-03
  0.100E+05   0.210E+03  0.999E-03  0.621E-03  0.696E-03  0.884E-03
  0.200E+01   0.225E+03  0.585E-03  0.384E-03  0.454E-03  0.444E-03
  0.299E+01   0.225E+03  0.606E-03  0.363E-03  0.455E-03  0.442E-03
  0.482E+01   0.225E+03  0.626E-03  0.344E-03  0.455E-03  0.442E-03
  0.875E+01   0.225E+03  0.638E-03  0.331E-03  0.451E-03  0.446E-03
  0.200E+02   0.225E+03  0.631E-03  0.330E-03  0.438E-03  0.455E-03
  0.807E+02   0.225E+03  0.606E-03  0.336E-03  0.416E-03  0.468E-03
  0.100E+05   0.225E+03  0.621E-03  0.431E-03  0.422E-03  0.621E-03
  0.200E+01   0.240E+03  0.556E-03  0.414E-03  0.452E-03  0.445E-03
  0.299E+01   0.240E+03  0.550E-03  0.377E-03  0.434E-03  0.424E-03
  0.482E+01   0.240E+03  0.526E-03  0.329E-03  0.401E-03  0.393E-03
  0.875E+01   0.240E+03  0.476E-03  0.274E-03  0.348E-03  0.353E-03
  0.200E+02   0.240E+03  0.394E-03  0.226E-03  0.274E-03  0.310E-03
  0.807E+02   0.240E+03  0.299E-03  0.195E-03  0.198E-03  0.278E-03
  0.100E+05   0.240E+03  0.276E-03  0.229E-03  0.174E-03  0.341E-03
  0.200E+01   0.255E+03  0.522E-03  0.448E-03  0.450E-03  0.447E-03
  0.299E+01   0.255E+03  0.492E-03  0.402E-03  0.418E-03  0.412E-03
  0.482E+01   0.255E+03  0.436E-03  0.335E-03  0.361E-03  0.357E-03
  0.875E+01   0.255E+03  0.345E-03  0.246E-03  0.276E-03  0.281E-03
  0.200E+02   0.255E+03  0.222E-03  0.152E-03  0.166E-03  0.194E-03
  0.807E+02   0.255E+03  0.103E-03  0.821E-04  0.660E-04  0.121E-03
  0.100E+05   0.255E+03  0.567E-04  0.689E-04  0.264E-04  0.114E-03
  0.200E+01   0.270E+03  0.485E-03  0.485E-03  0.449E-03  0.449E-03
  0.299E+01   0.270E+03  0.442E-03  0.442E-03  0.410E-03  0.410E-03
  0.482E+01   0.270E+03  0.370E-03  0.370E-03  0.346E-03  0.346E-03
  0.875E+01   0.270E+03  0.266E-03  0.266E-03  0.252E-03  0.252E-03
  0.200E+02   0.270E+03  0.143E-03  0.143E-03  0.140E-03  0.140E-03
  0.807E+02   0.270E+03  0.388E-04  0.388E-04  0.420E-04  0.420E-04
  0.100E+05   0.270E+03  0.198E-05  0.198E-05  0.690E-05  0.690E-05
```



☆ U S GOVERNMENT PRINTING OFFICE 1982—576-001/1233 REGION No. 8

# Environmental Research LABORATORIES

**The mission of the Environmental Research Laboratories (ERL) is to conduct an integrated program of fundamental research, related technology development, and services to improve understanding and prediction of the geophysical environment comprising the oceans and inland waters, the lower and upper atmosphere, the space environment, and the Earth. The following participate in the ERL missions:**

**AL** *Aeronomy Laboratory.* Studies the physics, dynamics, and chemistry of the stratosphere and the surrounding upper and lower atmosphere.

**AOML** *Atlantic Oceanographic and Meteorological Laboratories.* Study the physical, chemical, biological, and geological characteristics and processes of the ocean waters, the sea floor, and the atmosphere above the ocean, including tropical meteorology such as hurricanes and tropical weather systems.

**ARL** *Air Resources Laboratories.* Study the diffusion, transport, dissipation, and chemistry of atmospheric pollutants; develop methods of predicting and controlling atmospheric pollution; monitor the global physical environment to detect climatic change.

**GFDL** *Geophysical Fluid Dynamics Laboratory.* Studies the dynamics of geophysical fluid systems (the atmosphere, the hydrosphere, and the cryosphere) through theoretical analysis and numerical simulation using powerful, high-speed digital computers.

**GLERL** *Great Lakes Environmental Research Laboratory.* Studies hydrology, waves, currents, lake levels, biological and chemical processes, and lake-air interaction in the Great Lakes and their watersheds; forecasts lake ice conditions.

**NSSL** *National Severe Storms Laboratory.* Studies severe-storm circulation and dynamics, and develops techniques to detect and predict tornadoes, thunderstorms, and squall lines.

**OWRM** *Office of Weather Research and Modification.* Conducts a program of basic and applied research to advance the understanding and define the structure of mesoscale phenomena, to improve short-range weather predictions and warnings, and to identify and test hypotheses for beneficially modifying weather processes.

**PMEL** *Pacific Marine Environmental Laboratory.* Monitors and predicts the physical and biochemical effects of natural events and human activities on the deep-ocean and coastal marine environments of the Pacific region.

**PROFS** *Prototype Regional Observing and Forecasting Service.* Evaluates and integrates advanced meteorological measurement, forecasting, and communication/dissemination technologies into functional mesoscale weather forecast system designs for transfer to operational agencies such as NWS, NESS, and FAA.

**RFC** *Research Facilities Center.* Operates instrumented aircraft for environmental research programs; provides scientific measurement tools, logged data, and associated information for meteorological and oceanographic research programs.

**SEL** *Space Environment Laboratory.* Studies solar-terrestrial physics (interplanetary, magnetospheric, and ionospheric); develops techniques for forecasting solar disturbances; provides real-time monitoring and forecasting of the space environment.

**WIM** *Weather Modification Program Office.* Plans and coordinates ERL weather modification projects for precipitation enhancement and severe storms mitigation.

**WPL** *Wave Propagation Laboratory.* Develops, and applies to research and services, new methods for remote sensing of the geophysical environment.

**U.S. DEPARTMENT OF COMMERCE**
**National Oceanic and Atmospheric Administration**
BOULDER, COLORADO 80302